Ice multiplication from ice-ice collisions in the high Arctic: sensitivity to ice habit, rimed fraction, ice type and uncertainties in the numerical description of the process

Georgia Sotiropoulou[1,2], Luisa Ickes[3], Athanasios Nenes[2,4] and Annica M. L. Ekman[1]

[1]Department of Meteorology, Stockholm University & Bolin Center for Climate Research, Stockholm, Sweden

[2]Laboratory of Atmospheric Processes and their Impacts, School of Architecture, Civil & Environmental Engineering, Ecole Polytechnique Fédérale de Lausanne, Lausanne, Switzerland

[3]Department of Space, Earth and Environment, Chalmers University of Technology, Gothenburg, Sweden

[4]Institue for Chemical Engineering Sciences, Foundation for Research and Technology Hellas, Patras, Greece

Correspondence: georgia.sotiropoulou@misu.su.se

Abstract. Atmospheric models often fail to correctly reproduce the microphysical structure of Arctic mixed-phase clouds and underpredict ice water content, even when the simulations are constrained by observed levels of ice nucleating particles. In this study we investigate whether ice multiplication from break-up upon ice-ice collisions, a process missing in most models, can account for the observed cloud ice in a stratocumulus cloud observed during the Arctic Summer Cloud Study campaign. Our results indicate that the efficiency of this process in these conditions is weak; increases in fragment generation are compensated by subsequent enhancement of precipitation and subcloud sublimation. Activation of collisional break-up improves the representation of cloud ice content, but cloud liquid remains overestimated. In most sensitivity simulations, variations in ice habit and prescribed rimed fraction have little effect on the results. A few simulations result in explosive multiplication and cloud dissipation; however, in most set-ups, the overall multiplication effects become substantially weaker if the precipitation sink is enhanced through cloud ice-to-snow autoconversion. The largest uncertainty stems from the correction factor for ice enhancement due to sublimation included in the break-up parameterization; excluding this correction results in rapid glaciation, especially in simulations with plates. Our results indicate that the lack of a detailed treatment of ice habit and rimed fraction in most bulk microphysics schemes is not detrimental for the description of collisional break-up process in the examined conditions, as long as cloud ice-to-snow autoconversion is considered.

Introduction

Cloud feedbacks play an important role in Arctic climate change (Cronin and Tziperman, 2015; Kay et al., 2016; Tan and Storelvmo, 2019) and sea-ice formation (Burt et al., 2015; Cao et al., 2017). However, despite their significant climatic impact, Arctic mixed-phase clouds remain a great source of uncertainty in climate models (Stocker et al., 2013; Taylor et al., 2019). To accurately predict the radiative effects of mixed-phase clouds in models, an adequate description of their microphysical structure, such as the amount and distribution of both liquid water and ice, is required (Korolev et al., 2017). Both ice nucleation and liquid drop formation require seed particles to be present known as ice nucleating particles (INPs) and cloud condensation nuclei CCN), respectively. However, the observed ice crystal number concentrations (ICNCs) are often much higher than the observed INP concentrations in the Arctic (Fridlind et al., 2007; 2012; Gayet et al., 2009; Lloyd et al., 2015), where INPs are generally sparse (Wex et al., 2019). Moreover, model simulations constrained by INP measurements frequently underpredict the observed amount of ice (Fridlind and Ackerman, 2019).

Secondary Ice Processes (SIP) have been suggested as the reason why ice crystal concentrations exceed INP levels (Field et al., 2017; Fridlind and Ackerman, 2019). SIP involve the production of new ice crystals in the presence of pre-existing ice, without requiring the presence of an INP. The most well-known mechanism is rime-splintering (Hallet and Mossop, 1974), which refers to the ejection of ice splinters when ice particles collide with supercooled liquid drops. Rime-splintering is active only in a limited temperature range, between -8°C and -3°C, and requires the presence of liquid droplets both smaller than 13 μm and larger than 25 μm (Hallett and Mossop, 1974; Choularton et al., 1980). Moreover, recent studies have shown that rime-splintering alone cannot explain the observed ICNCs in polar clouds even within the optimal temperature range (Young et al., 2019; Sotiropoulou et al., 2020a,b). Ice fragments may also be generated when a relatively large drop freezes and shatters (Lauber et al., 2018; Phillips et al., 2018); drop-shattering, however, has been found insignificant in polar conditions (Fu et al., 2019; Sotiropoulou et al., 2020). Finally, ice multiplication can occur from mechanical break-up due to ice-ice collisions (Vardiman et al., 1978; Takahashi et al., 1995). This process has been also identified in in-situ measurements of Arctic clouds (Rangno and Hobbs, 2001; Schwarzenboeck et al., 2009).

Schwarzenboeck et al. (2009) found evidence of crystal fragmentation in 55% of in-situ observations of ice particles collected with a Cloud Particle Imager during ASTAR (Arctic Study of Aerosols, Clouds and Radiation) campaign. However, natural fragmentation could only be confirmed for 18% of these cases, which was identified by either subsequent growth near the break area or/and lack of a fresh break-up line (which indicates toward shattering on the probe). For the rest of their samples, artificial fragmentation could not be excluded. Moreover, their analysis included only crystals with

stellar shape and sizes round 300 μm or roughly larger. This suggests that the frequency of collisional break-up in Arctic clouds is likely higher in reality compared to what is indicated in their study. Yet, despite the potential impact of this process in Arctic conditions, it has received little attention from the modeling community.

Fridlind et al. (2007) and Fu et al. (2019) investigated the contribution from ice-ice collisions in an autumnal cloud case observed during the Mixed-Phase Arctic Cloud Experiment (M-PACE) and found that the process could not account for the observed ice content at in-cloud temperatures between -8.5^{o}C and -15.5^{o}C. The parameterization of the break-up process used in these studies was based on the laboratory data of Vardiman (1978). However, there are significant shortcomings in the available laboratory measurments. For example, in Vardiman (1978) the ice particles were collected in a mountainside below cloud base, thus the collected samples were impacted by sublimation. Takahashi et al. (1995) also used an unrealistic set-up: they performed collisions between cm-size hailballs, while one of the colliding hydrometeors was unrimed and fixed. These considerations preclude deriving an accurate parameterization for ice multiplication due to collisional break-up from this data alone.

Phillips et al. (2017a,b) developed a more advanced treatment of ice multiplication from ice-ice collisions, which is based on the above mentioned laboratory results, but further considers the impact of collisional kinetic energy, ice habit, ice type and rimed fraction. More specifically, their parameterization accounts for dendritic and non-dendritic planar ice shapes; the latter includes plates, columns and needles, thus all the ice habits for which there are no available observations of break-up. Moreover, to correct the effect of sublimation in Vardiman's (1978) data, they adjusted the fragile coefficient (term ψ in Appendix A) in their description. While these approximations are a source of uncertainty, their parameterization has been tested in polar clouds (Sotiropoulou et al. 2020; 2021) and resulted in ice enhancements that could explain the observed ICNCs. Sotiropoulou et al. (2020; 2021) focused on relatively warm polar clouds (-3°C to -8°C), for which rime-splintering is considered to be the dominant SIP mechanism; yet the efficiency of this process alone was found to be limited in these studies. In Sotiropoulou et al. (2020) the combination of both rime-splintering and collisional break-up was essential to explain observed ICNCs, while in Sotiropoulou et al. (2021) rime-splintering had hardly any impact. Zhao et al. (2021) however found limited efficiency of this process in Arctic clouds with cloud-top temperatures between -10°C and –15°C, while other formation processes (heterogeneous freezing and drop-shattering) appeared more important.

In this study, we aim to investigate the role of ice-ice collisions in high-Arctic clouds with cloud-top temperatures -9.5^{o}C to –12.5^{o}C; a temperature range for which previous studies found limited efficiency of the process (Fridlind et al., 2007; Fu et al., 2019; Zhao et al. 2021). The Phillips parameterization is implemented in the MIT-MISU Cloud-Aerosol (MIMICA) Large Eddy Simulation

(LES) model to examine its performance for a stratocumulus case observed during the Arctic Summer Cloud Study (ASCOS) campaign in the high Arctic. To identify the optimal microphysical conditions for ice multiplication through collisional break-up, the sensitivity of the results to the assumed rimed fraction, ice habit and ice type (e.g. cloud ice/ snow) of the colliding ice particles is examined.

2. Field observations

The ASCOS campaign was deployed on the Swedish icebreaker *Oden* between 2 August and 9 September 2008 in the Arctic Ocean, to improve our understanding of the formation and life-cycle of Arctic clouds. It included an extensive suite of in-situ and remote sensing instruments, a description of which can be found in Tjernström et al. (2014). Here we only offer a brief description of the instruments and measurements utilized in the present study.

2.1. Instrumentation

Information on the vertical atmospheric structure was derived from Vaisala radiosondes, released every 6 hours, with 0.15^{o}C and 3% uncertainty in temperature and relative humidity profiles, respectively. Cloud boundaries were derived from a vertically-pointing 35 GHz Doppler Millimeter Cloud Radar (MMCR; Moran et al., 1998) with a vertical resolution of 45 m and two laser ceilometers. CCN concentrations were measured by an in-situ CCN counter (Roberts and Nenes, 2005), set at a constant supersaturation of 0.2% (with an uncertainty of ±0.04%; Moore et al. 2011) based on typical values used in other similar expeditions (Bigg and Leck, 2001; Leck et al., 2002). The total uncertainty in CCN concentration derived from counting statistics and fluctuations in pressure and flow rate is 7–16% for CCN concentrations above 100 cm^{-3} (Moore et al., 2011). Vertically-integrated liquid water path (LWP) was retrieved from a dual-channel microwave radiometer, with an uncertainty of 25 g m^{-2} (Westwater et al., 2001). Ice water content (IWC) was estimated from the radar reflectivity observed by the MMCR, using a power-law relationship (e.g. Shupe et al, 2005), with a factor of 2 uncertainty; The ice water path (IWP) was integrated from the IWC estimates.

2.2. ASCOS case study

A detailed description of the conditions encountered during the ASCOS campaign is available in Tjernström et al. (2012). Our focus here is on a stratocumulus deck observed between 30-31 August, while *Oden* was drifting with a 3×6 km^2 ice-floe at approximately $87^{°}$ N. During that time, relatively quiescent large-scale conditions prevailed, characterized by a high-pressure system and large-scale subsidence in the free troposphere and only weak frontal passages (Tjernström et al., 2012).

Our simulations are initialized with thermodynamic and cloud liquid profiles representing conditions observed on 31 August at 06 UTC (Fig. 1). These profiles display a cloud layer between 550 and 900 m above ground level (a.g.l), at temperatures between -7°C and -10°C, capped by a temperature and humidity inversion, of about 5°C and 0.5 g kg^{-1}, respectively. A weak secondary temperature inversion is also observed at about 370 m a.g.l., indicating that the cloud is decoupled from the surface; this type of vertical structure, with a decoupled surface and cloud layer, dominated during the whole ASCOS experiment (Sotiropoulou et al., 2014). More generally, this case study is representative of typical cloudy boundary layers over sea-ice, where co-existing temperature and humidity inversions are frequently observed (Sedlar et al., 2012), and clouds are often decoupled from any surface sources of e.g. moisture (Sotiropoulou et al., 2014).

The observed cloud layer remained 'stable' for about 12 hours prior to the selected profile and began dissipating after 31 August 9 UTC. A substantial reduction in the background aerosol concentration has been suggested as a possible cause for the sudden collapse of the cloud layer, which cannot be simulated by models without prognostic aerosol processes (Stevens et al., 2018). For this reason, we will use observational statistics from the period with the persistent stratocumulus conditions to evaluate our results, although simulations are allowed to run for 24 hours in a quasi-equilibrium state.

3. Model and Methods

3.1. LES set-up

The MIMICA LES (Savre et al., 2014) solves a set of non-hydrostatic prognostic equations for the conservation of momentum, ice-liquid potential temperature and total water mixing ratio with an anelastic approximation. A fourth order central finite-differences formulation determines momentum advection and a second order flux-limited version of the Lax-Wendroff scheme (Durran, 2010) is employed for scalar advection. Equations are integrated forward in time using a second order Leapfrog method and a modified Asselin filter (Williams, 2010). Subgrid scale turbulence is parameterized using the Smagorinsky-Lilly eddy-diffusivity closure (Lilly, 1992) and surface fluxes are calculated according to Monin-Obukhov similarity theory.

MIMICA employs a bulk microphysics scheme with a two-moment approach for cloud droplets, rain and cloud ice, graupel and snow particles. Mass mixing ratios and number concentrations are treated prognostically for these five hydrometeor classes, whereas their size distributions are defined by generalized Gamma functions. Cloud droplet and raindrop processes follow Seifert and Beheng (2001), while liquid/ice interactions are parameterized as in Wang and Chang (1993). Collisions between cloud ice larger than 150 μm and droplets larger than 15 μm, or raindrops, result in graupel formation; the efficiency of this conversion increases with increasing ice particle size. Graupel is also formed when

snow and liquid particle collisions occur. These liquid particles can also be directly collected by graupel. Self-aggregation of cloud ice particles result in snow; this is the only snow formation mechanism in the default microphysics scheme. Self-aggregation is also allowed between snow particles, droplets larger than 15 μm and rain; aggregated snow particles and droplets are converted to graupels and raindrops, respectively. A simple parameterization for CCN activation is applied (Khvorostyanov and Curry, 2006), where the number of cloud droplets formed is a function of the modeled supersaturation and a prescribed background aerosol concentration. A detailed radiation solver (Fu and Liou, 1992) is coupled to MIMICA to account for cloud radiative properties when calculating the radiative fluxes.

The model configuration adopted is based on Ickes et al. (in prep.), who simulated the same case to examine the performance of various primary ice nucleation schemes. All simulations are performed on a 96×96×128 grid, with constant horizontal spacing $dx = dy = 62.5$ m. The simulated domain is 6×6 km^2 horizontally and 1.7 km vertically. At the surface and in the cloud layer the vertical grid spacing is 7.5 m, while between the surface and the cloud base it changes sinusoidally, reaching a maximum spacing of 25 m. The integration time step is variable (~ 1-3 sec), calculated continuously to satisfy the Courant-Friedrichs-Lewy criterion for the Leapfrog method. While this approach prevents numerical instabilities, its dynamic nature does not allow sensitivity simulations to be performed with exactly the same timestep. Lateral boundary conditions are periodic, while a sponge layer in the top 400 m of the domain dampens vertically-propagating gravity waves generated during the simulations. To accelerate the development of turbulent motions, the initial ice-liquid potential temperature profiles are randomly perturbed in the first 20 vertical grid levels with an amplitude less than 3×10^{-4} K.

Surface pressure and temperature are set to 1026.3 hPa and -3.2°C, respectively, constrained by surface sensors deployed on the ice-pack. The surface moisture is set to the saturation value, which reflects summer ice conditions. The surface albedo is assumed to be 0.85, which is representative of a multi-year ice pack. In MIMICA, subsidence is treated as a linear function of height: $w_{LS} = -D_{LS} \cdot z$, where D_{LS} is set 1.5×10^{-6} s^{-1} and z is the height in meters. Finally, the prescribed number of CCN is set to 30 cm^{-3} over the whole domain, which represents mean accumulation mode aerosol concentrations observed during the stratocumulus period (Igel et al., 2017). The duration of all simulations is 24 hours, where the first 4 hours constitute the spin-up period.

3.2 Ice Formation Processes in MIMICA

3.2.1 Primary ice production

Ickes et al. (in prep.) recently implemented several primary ice production (PIP) schemes in MIMICA. Here, we utilize the empirical ice nucleation active site density parameterization for

immersion freezing, which is based on Connolly et al. (2009) and was further developed by Niemand et al. (2012) for Saharan dust particles. This formulation was used by Ickes et al. (2017) to describe the freezing behavior of different dust particle types, including microline (Appendix A). Microcline is a feldspar type that is known to be an efficient INP (Atkison et al., 2013). As no aerosol composition (or INP) measurements are available for the ASCOS campaign, we will use this INP type as a proxy for an aerosol constituent that can produce primary ice at the relatively warm sub-zero temperatures (-7°C to -10°C) of the initial observed cloud profile (Fig. 1a). At these temperatures it is reasonable to assume that most of the PIP occurs through immersion freezing (Andronache, 2017), i.e. that an aerosol must be both CCN active and contain ice-nucleating material to initiate ice production. Thus, we will simply assume that a specified fraction of the CCN population contains some efficient ice-nucleating material, here represented as feldspar, and match this fraction so that the model simulates reasonable values of LWP, IWP and ICNC (Appendix A, Text S1). Based on this procedure, we infer that the CCN population contains 5% microline, a value that results in realistic primary ICNCs (Wex et al., 2019), but in an underestimate of the IWP and an overestimate of the LWP (Text S1, Fig. S1). Note that even though we assume this relatively high fraction of ice-nucleating material (Text S1, Fig. S1), MIMICA still underestimates the IWP; we postulate that omitting the effects of secondary ice production may be the reason for this bias.

3.2.2 Ice multiplication from ice-ice collisions

The observed in-cloud temperatures are generally below the rime-splintering temperature range, except for the somewhat warmer temperatures near cloud base (Fig. 1a). Some studies indicate that drop-shattering is ineffective in Arctic conditions (Fu et al., 2019; Sotiropoulou et al., 2020a), while Zhao et al.(2021) have found significant contribution from this process. Nevertheless, our simulations suggest inefficiency of both these mechanisms in the examined conditions, as the concentration of large raindrops is too low (below 0.1 cm^{-3}) to initiate them (Fig. S1c). Hence we focus solely on ice multiplication from ice-ice collisions.

We implement the parameterization developed by Phillips et al. (2017a) in MIMICA and allow for ice multiplication from cloud ice-cloud ice, cloud ice-graupel, cloud ice-snow, snow-graupel, snow-snow and graupel-graupel collisions (Appendix B). The generated fragments are considered "small ice" crystals and are added to the cloud ice category in the model. The Phillips parameterization explicitly considers the effect of ice type, ice habit and rimed fractions of the colliding particles on fragment generation (Appendix B). The sensitivity of the model performance to these parameters is examined through sensitivity simulations. Additional tests are also performed to quantify the sensitivity to other

sources of uncertainty, such as the applied correction for the sublimation effects in Vardiman's (1978) data (see section 1) and the estimated number of fragments.

3.3 Sensitivity simulations

A detailed description of the sensitivity tests is provided in this section, while a summary is offered in Table 2.

3.3.1 The role of ice habit

Cloud ice observed within the examined temperature range can either be shaped as a dendrite or a plate, depending on the supersaturation with respect to ice (Pruppacher and Klett, 1997). However, as the mean vapor density excess in the simulated cloud layer varies between 0.03 and 0.22 g m^{-3}, it is not clear which shape should theoretically dominate (Pruppacher and Klett, 1997). Moreover, observations often indicate variable shapes within the same temperature conditions (Mioche et al., 2017). The formulation for ice multiplication due to break-up is substantially different for these two ice habits, with plates being included in the non-dendritic planar ice category (Appendix B).

MIMICA allows for variable treatment of the ice habit for the cloud ice category. These variations correspond to different characteristic parameters in the ($m = a_m D^{bm}$) and fallspeed-diameter ($v = a_v D^{bv}$) relationships (Table 2). To test the sensitivity of our results to the assumed cloud ice habit, the two simulations CNTRLDEN and CNTRLPLA are performed. 'CNTRL' refers to simulations that account only for PIP, while the suffixes 'DEN' and 'PLA' indicate dendritic and and non-dendritic planar cloud ice shape, respectively. Note that particle properties in CNTRLPLA simulations are adapted for plates (Pruppacher and Klett 1997), while the non-dendritic planar category in the Phillips parameterization encompasses a larger range of shapes (columns, needles, etc.).

Characteristic parameters for graupel in the default MIMICA version are relatively large, with a_v being one order of magnitude larger than the values adapted in other stratocumulus schemes (e.g. Morrison et al 2005). This difference has a weak impact on simulations that do not account for collisional break-up. However if break-up is active, fragment generation is a function of colliosional kinetic energy and the results become more sensitive to the choice of these parameters. Since Arctic clouds are characterized by weak convective motions and the formation of large rimed particles is not favored, the characteristic parameters of graupel are adjusted following Morrison et al. (2005) (Table 2).

3.3.2 The role of rimed fraction

F_{BR} is parameterized as a function of the rimed fraction (Ψ) of the ice crystal or snowflake that undergoes break-up; fragment generation from break-up of graupel does not depend on Ψ (see Appendix

B). This parameter is not explicitly predicted in most bulk microphysics schemes, but can substantially affect the multiplication efficiency of the break-up process (Sotiropoulou et al., 2020a). For this reason, we will consider values of Ψ for cloud ice and snow between 0.1 (lightly rimed) and 0.4 (heavily rimed) (Phillips et al., 2017a, b); graupel particles are considered to have $\Psi \geq 0.5$. Both Sotiropoulou et al. (2020) and (2021) found that ice multiplication in polar clouds at temperatures above -8°C is initiated only when a highly rimed fraction of cloud ice and snow is assumed. Their conclusions however may not be valid for our case, as the temperature and microphysical conditions are substantially different.

The effect of varying Ψ is examined for the two ice habits that prevail in the observed temperature range (Section 3.2.2). The performed simulations are referred to as BRDEN0.1, BRDEN0.2, BRDEN0.4, and BRPLA0.1, BRPLA0.2 BRPLA0.4, for dendrites and plates respectively (see Table 3). 'BR' indicates that collisional break-up is active, while the number 0.1-0.4 corresponds to the assumed value of Ψ. Note that assuming a constant rimed fraction for cloud ice and snow is unrealistic; this variable depends both on size and temperature. Yet the performed test will reveal whether a more realistic treatment of Ψ is essential for the description of collisional break-up. This information is useful particularly for implementations in climate models, where rimed fraction is not predicted and minimizing the computational cost of microphysical processes is important.

3.3.3 The impact of the ice hydrometeor type

The MIMICA LES has previously been used to study ice-ice collisions in Sotiropoulou et al. (2020), however, they used a parcel-model-based parameterization of the process, instead of implementing a break-up parameterization as a part of the MIMICA microphysics scheme. Sotiropoulou et al. argued that the efficiency of the process is likely underestimated in bulk microphysics schemes, where the dynamics of the ice particle spectrum is poorly represented and fixed particle properties are assumed typically for three ice types (cloud ice, graupel, snow), which is rather unrealistic. Their argument might be particularly true for the studied case where no snow is produced in the simulations with dendrites (Fig. S1d).

An interesting finding in Stevens et al. (2018), who compared the performance of several models that simulated the present case, was that the dominant ice particle type can be highly variable among the different models. For example, COSMO-LES and the Weather and Reseach Forecasting (WRF) model contain only a single ice particle category, which is cloud ice and snow respectively. MIMICA simulates both graupel and cloud ice, with former being substantially more abundant for the present case. COSMO-NWP (numerical weather prediction model) and UM-CASIM (the Met Office Unified Model with Cloud AeroSol Interacting Microphysics model) simulate snow and cloud ice. Cloud ice number concentrations were very limited in COSMO-NWP, while they were comparable to snow concentrations

in UM-CASIM. These differences in ice particle properties result in very different ice water content (IWC) (see Fig. 11 in Stevens et al. (2018)) and can likely affect the efficiency of the break-up process. Nevertheless, MIMICA is the model that predicts more realistic IWC values in the study by Stevens et al. (2018), while most models (except UM-CASIM) predict very little ice content.

The main reason why MIMICA favors graupel formation is because all cloud ice particles with sizes larger than 150 μm that collide with droplets are added to this category. This is not the same in other schemes (e.g. Morrison et al., 2005) who considers that once cloud droplets are accreted on cloud ice, the rimed particle remains in the same ice category. However adapting this approach in our model resulted in substantial enhancement of the cloud ice content and eventually to cloud glaciation (not showed). This indicates that different bulk microphysics schemes are tuned in very different ways. Another difference is that MIMICA allows for snow formation only through aggregation of cloud ice particles, while other microphysics schemes (Morrison et al., 2005; Morrison and Gettelman, 2008) also consider that cloud ice particles can grow to snowflakes through vapor deposition.

To test how differences in cloud ice content distribution among different hydrometeor types affect the multiplication efficiency of break-up, we further implemented a description for cloud ice-to-snow autoconversion (Appendix C) assuming that ice crystals with diameters larger than 500 μm are converted to snow. These simulations are referred to as: CNTRLDENauto, BRDEN0.2auto, BRDEN0.4auto for dendritic cloud ice/snow and CNTRLPLAauto, BRPLA0.2auto, BRPLA0.4auto when a non-dendritic planar ice habit is assumed. The number 0.2 or 0.4 indicates the prescribed rimed fraction. Tests with a lower separation diameter for cloud ice and snow showed little sensitivity to the choice of this parameter. In addition to the cloud ice-to-snow autoconversion description given in Appendix C, we also tested a different parameterization following Ferrier et al. (1994). In order to conserve the highest moments of the ice particle spectra, this parameterization assumes that the number of cloud ice are approximately constant by converting a few large ice crystals into snow. Yet, activating this process had very little impact on the macrophysical properties in simulations with inactive and active BR. While the results of this set of simulations are not shown, the reasons for a variable sensitivity to different descriptions of the autoconversion process are discussed in the text.

3.3.4 The impact of sublimation correction factor

As already discussed in section 1, the laboratory data used to develop the existing parameterization (Vardiman 1978; Takahashi et al. 1995) for break-up do not represent realistic in-cloud conditions. Phillips et al. (2017a) have attempted to quantify the impact of the simplifications in the laboratory set-ups. However, there is still significant uncertainty in the developed parameterization. For example, the correction factor induced in the fragility coefficient to account for the effects of sublimation on

Vardiman's (1978) data was derived by the measurements of Takahashi et al. (1995) which were performed in near saturated conditions. This factor is thus highly uncertain and can substantially reduce the number of generated fragments (see Figs. 4-6 in Phillips et al. 2017a). To test the impact of this empirical correction, two simulations are perfomed in which this factor has been removed from the BR parameterization. These are referred as BRDENsub and BRPLAsub in the text (see Table 3). Finally, this modification is tested in conditions with enhanced snow formation, which are imposed by activating the cloud ice-to-snow autoconversion process (see section 3.3.3): these additional tests are referred as BRDENsubauto and BRPLAsubauto (Table 3). The rimed fraction in all these set-ups is set to 0.2.

4. Results

4.1 Sensitivity to ice habit and rimed fraction

The impact of the assumed ice habit and rimed fraction in the predicted liquid and ice water path (LWP, IWP) is presented in Fig. 2, while the median and interquartile statistics are summarized in Table 4. To quantify break-up efficiency, fragment generation rates (*PBR*) for the different collision types are shown in Fig. 3 (see Appendix B for detailed formulas). *PBR* results are only presented for cloud ice-graupel, graupel-snow and snow-snow collisions since we find negligible contributions from cloud ice-cloud ice, cloud ice-snow and graupel-graupel collisions.

Small differences are observed in the integrated cloud water quantities between CNTRLDEN and CNTRLPLA, as both produce median LWP values between 139-143 g m^{-2} and median IWP values of 1.8-2.2 g m^{-2}. Hence, both simulations overestimate cloud liquid (Fig. 2a-b) and underestimate ice compared to observations (Fig. 2c-d). Specifically, the median observed LWP (73.8 g m^{-2}) is overestimated by almost a factor of two, while IWP (7 g m^{-2}) is underestimated by about a factor of 3-3.5 (Table 4), which is larger than the uncertainty in the observations.

Activating break-up for dendrites results in improved simulated water properties: median LWP (IWP) decreases (increases) by 32-36 (2.2-3.8) g m^{-2}, with differences in the assumed rimed fraction having a weak impact on the results (Fig. 2a, c). The total fragment generation rates in Fig. 3 indicate that ice multiplication is dominated by snow-graupel collisions in these simulations. It is interesting that while snow is not formed in the CNTRLDEN simulation (Fig. S2), activation of break-up enhances cloud ice concentrations and thus the frequency of collisions between them, which promotes snow formation; break-up of snow eventually dominates the multiplication process (Fig. 3a,c,d). Generally, all total fragmentation rates in simulations with dendrites remain below 1.1 (L^{-1} s^{-1}), with small differences for different assumptions in Ψ (Fig. 3a,c,d).

Simulations with plates and a rimed fraction <= 0.2 produce similar macrophysical properties (Fig. 2b, d); LWP (IWP) decreases (increases) by 20-25 (2.4-2.6) g m^{-2}, suggesting lower efficiency of break-up compared to simulations with dendrites. This is also indicated by the lower fragment generation rates, which reach a maximum value of 0.8 (L^{-1} s^{-1}) at the end of BRPLA0.1 and BRPLA0.2 simulations (Fig. 3b,d,e). However, the cloud in BRPLA0.4 rapidly dissipates after 8 hours owing to excessive multiplication, with the total P_{BR} reaching a maximum of 12.8 L^{-1}s^{-1} (Fig. 5b,d,f). Yet, a supercooled-liquid cloud reforms after 15 hours; LWP increases again to values larger than 100 g m^{-2} by the end of the simulated period (Fig. 2b), while IWP remains close to zero (Fig. 2d). Our findings are in agreement with Loewe et al. (2018) who showed that a prescribed ICNC value of 10 L^{-1} can lead to cloud dissipation for the specific case study.

Analysis of the simulation results indicates strong feedbacks between fragment generation, precipitation and evaporation/sublimation within the subcloud layer. To facilitate the discussion of these feedbacks, timeseries of mean surface precipitation rates and minimum sub-cloud saturation values are presented in Fig. 4, while the relative frequency distributions (RFD) of the charactrestic diameters of cloud ice and snow particles are shown in Fig. 5. Precipitation rates increase when break-up is activated (Fig. 4a-b), resulting in an overall lower total condensate. Moreover, saturation with respect to both liquid (Fig. 4c-d) and ice (Fig. 4e-f) decrease in all these simulations, except in BRPLA0.4, as increasing precipitation depletes the available water-vapor in the subcloud layer. This process further enhances the reduction of the total water path (LWP+IWP). An opposite behaviour is only found in BRPLA0.4 (Fig. 5d, f); the continuous multiplication shifts ice particle distributions to substantially smaller sizes (Fig. 5b, d), that can sublimate more efficiently in the sub-cloud layer. The feedbacks between break-up efficiency and changes in the simulated particle size distributions are discussed in more detail below.

Offline estimates of the cloud ice and snow diameters, calculated from the domain-averaged concentration profiles, are shown in Fig. 5. The RFDs of the cloud ice diameter exhibit a bimodal distribution for all simulations with dendrites (Fig. 5a). This is due to fact that cloud ice-to snow autoconversion is not treated in the default MIMICA model and ice crystals are allowed to grow to precipitation sizes without any size limits. Such precipitation-sized particles are represented by the second mode that corresponds to a size range similar to that for snow particles (Fig. 5c). The first mode of the cloud ice RFD does not play a significant role in the ice multiplication process due to the small sizes ~200-250 μm; this is proven by the fact that the characteristics of this mode do not change among the different simulations. On the contrary, with increasing rime fraction and thus increasing fragment generation, the second mode (that undergoes break-up) shifts to smaller sizes. While the assumption of a constant Ψ for this rather broad RFD is unrealistic, the fact that only a certain size range of cloud-ice undergoes break-up makes this simplification more reasonable. Also the comparable sizes of this cloud

ice mode with snowflakes justify the adaption of the same Ψ for both ice types. Moreover, the increased fragment generation due to increasing Ψ is likely partly compensated by the the shift to smaller cloud ice and snow sizes, which are in turn expected to generate less fragments; this may explain the comparable fragmentation rates for all BRDEN set-ups (Fig. 3a,c,e).

410   The above conclusions also hold for simulations with plates and $\Psi<=0.2$. In BRPLA0.4 the fragment generation completely changes the RFD shape, resulting in a monomodal distribution with a substantially narrower range (Fig. 5b). Now all cloud particles can contribute to multiplication while they are not efficiently depleted by precipitation, resulting in an explosive ice production. Thus for such large changes in the shape of the RFD, the assumption of a constant Ψ throughout the simulation cannot
415 be held and overestimations of this property can result in significant errors in cloud representation (Fig. 2b, d). While some atmospheric models explicitly predict rimed fraction (Morrison and Milbrandt 2015), such a detailed treatment is unlikely to be adapted in coupled General Circulation Models (GCMs) where minimizing computational costs is critical.

         Generally, BR efficiency is found weak for the examined conditions, as ICNC enhancement
420 rarely exceeds a factor of 2 in most simulations (Fig. 6a, b). This is substantially lower than the 10-20fold enhancement found in Sotiropoulou et al. (2020, 2021) for warmer mixed-phase clouds. However, note that an ICNC increase larger than a factor of 10, as in BRPLA0.4, would lead to cloud glaciation in the examined conditions (Fig. 6b). Yet this 1.5-2fold ICNC enhancement (Fig. 6a, b) is qualitatively consistent with in-situ Arctic cloud observations by Rangno and Hobbs (2001) who found
425 that 35% of the observed ice particles where likely produced by fragmentation upon ice particle collisions. It is interesting that a weak ICNC increase can enhance IWP by a factor of ~5 and ~3.3 in simulations with dendrites (Fig. 6c) and plates (Fig. 6d), respectively; this enhancement becomes gradually weaker after twelve hours of simulation, stabilizing to a factor 2. This is likely due to a feedback between BR efficiency and ICNC concentrations; as ICNCs increase with time the size spectra
430 is shifted to smaller sizes characterized by lower break-up efficiency. Overall, activation of break-up results in realistic IWP, while small improvements are found in the liquid properties; LWP remains above the observed interquartile range (Fig. 2a-b). Stevens et al. (2018) showed that simulations with interactive aerosols produce less LWP for the examined case, compared to simulations with a fixed background CCN concentration. Thus deviations between the simulated and observed LWP could be
435 attributed to the simplified aerosol treatment, rather than to inadequacies in the representation of the break-up process.

4.2 Sensitivity to snow formation

Ice multiplication generally shifts cloud ice size distributions to smaller values. In simulations with moderate fragment generation, precipitation processes can balance continuous fragment generation due to break-up (Fig. 2). However, in BRPLA0.4 the larger fragment generation cannot be counterbalanced by precipitation, resulting in continuous accumulation of cloud ice particles within the cloud layer until the cloud glaciates. This is indicated by the lack of the bimodal shape in the RFD for BRPLA0.4 presented in Fig 5b. However, this behaviour can largely be supported by the fact that cloud-ice to snow autoconversion is not treated in the default MIMICA version, which can enhance snow formation and thus precipitation.

Activation of autoconversion in simulation set-ups that do not account for break-up has hardly any impact on IWP and LWP properties (Fig. 7). LWP and IWP statistics are similar between CNTRLPLA–CNTRPLAauto and CNTRLDEN–CNTRDENauto. The same holds for simulations with dendrites and active break-up. BRPLA0.2auto produces somewhat improved LWP (reduced by ~13 g m$^-$^{2} compared to BRPLA0.2, Table 2), while the improvements are substantially larger in BRPLA0.4auto. The hypothesis that the implementation of cloud ice-to-snow autoconversion in the model can prevent the cloud glaciation occurring in BRPLA0.4 is confirmed in this simulation and the produced LWP and IWP statistics are similar to BRPLA0.2auto. However, this behaviour is not the same for all autoconversion schemes: application of the formulation described in Ferrier et al. (1994) does not prevent cloud dissipation (not shown). This is because Ferrier et al. (1994) assume that only very few large ice crystals are converted to snow and that the number concentration in the cloud ice category remains unaffected. To prevent explosive multiplication in this set-up, a reduction in cloud ice number concentration is essential.

Note that while with active break-up the model still does not reproduce liquid/ice partitioning correctly, there are significant improvements compared to the standard code. While CNTRLDENauto fails completely to reproduce the relationship between LWP and IWP (Fig. 8a, b), activation of break-up results in a partial agreement between modeled and observed LWP-IWP fields (Fig. 8a,c,d). Improvements of liquid-ice partitioning are also evident in BRPLA0.2auto and BRPLA0.4auto compared to CNTRLPLAauto (Fig. 9), with BRPLA0.2auto being in better agreement with ASCOS observations. However, there are still significant deviations particularly in the representation of the liquid condensate which can be linked either to an underestimate in the ice production or to the simplified treatment of aerosols that act as CCN (Stevens et al. 2018).

4.3 Sensitivity to the sublimation correction factor

In section 4.1, simulations with plates were found more sensitive to increases in fragment generation induced by changes in the prescribed Ψ. In particular, ICNC enhancements of a factor of 10 resulted in

cloud glaciation (Fig. 6b). Here we further examine the sensitivity of the results to increased ice multiplication by removing the correction factor for sublimation effects adapted in the Phillips et al (2017a) parameterization. For lightly rimed particles (Ψ=0.2), the reduction in fragment generation induced by this factor is largely variable depending on the collision type (see Figs 4b and 5a in Phillips et al 2017b).

Both BRDENsub and BRPLAsub simulations result in explosive ice multiplication and cloud dissipation (Fig. 10). In BRDENsub the cloud almost disappears after 6.5 hours and reforms after 8.5 hours (Fig 10a). In BRPLAsub the cloud glaciates within four hours and cloud-free conditions prevail for the rest of the simulation time (Fig 10b). Activation of cloud ice-to-snow autoconversion for this set-up prevents ice explosion and cloud dissipation in the simulation with dendrites but not with plates. In BRPLAsubauto, the autconversion process only delays cloud glaciation by 3 hours. Overall, the removal of the correction factor results in poorer agreement with observations (Table 2). This indicates that while the determination of the correction factor is highly uncertain, its inclusion in the break-up parameterization is essential when applied to polar stratocumulus clouds, particularly in the case of non-dendritic planar ice. The high sensitivity that simulations exhibit to this parameter suggests that possible errors in the estimation of the correction factor can have a large impact on the multiplication effect predicted by Phillips et al. (2017) parameterization, particularly in conditions that favor the formation of non-dendritic planar ice.

5. Discussion

Ice formation processes in Arctic clouds are sources of great uncertainty in atmospheric models, often resulting in underestimation of the cloud ice content compared to observations. The poor representation of SIP has been suggested as the main cause behind this underestimation (Fridlind and Ackerman 2019), as rime-splintering is usually the only multiplication mechanism described in models. In-situ observations (Rangno and Hobbs, 1991; Schwarzenboeck et al., 2009) and recent modeling studies (Sotiropoulou et al. 2020; 2021) suggest that collisional break-up is likely critical in polar mixed-phase clouds. However, due to the limited availability of laboratory studies and the unrealistic set-ups utilized in them (Vardiman 1978; Takahashi et al. 1995), the parameterization of this process is particularly challenging. Phillips et al. (2017a,b) have recently developed a physically-based numerical description for collisional break-up, constrained with existing laboratory data. This scheme estimates the number of fragments as a function of collisional kinetic energy, environmental temperature, size and rimed fraction of particle that undergoes break-up, while the influence of the different ice types and ice habits are also accounted.

While being more advanced than any other description for collisional break-up (e.g. Sullivan et al. 2018), the details of this parameterization cannot be addressed in most bulk microphysics schemes. While microphysics schemes with explicit prediction of the ice habit (e.g. Jensen et al 2017) or rimed fraction (e.g. Morrison and Milbradt 2015) have been developed, such detailed treatments are not utilized in coupled climate models as computational cost must be minimized. Thus the representation of break-up process in these models requires some simplifications. In this study we attempt to quantify the impact of ice multiplication through collisional break-up in summertime high-Arctic conditions and examine the sensitivity of the efficiency of this process to assumptions in the ice habit and rimed fraction of the colliding particles. We also examine how changes in ice type affect the multiplication process through activation of cloud-ice to snow autoconversion, a process not represented in the default model.

Simulations with a dendritic ice habit produce a realistic IWP when break-up is activated. The results show little sensitivity to assumptions in rimed fraction, suggesting that the lack of a prognostic treatment of this parameter in most bulk microphysics schemes is not detrimental for the description of the break-up process. Note that increases in Ψ result in increased ice multiplication that shifts the ice particle size distribution towards smaller values. These smaller particles can generate fewer fragments, which compensates for the enhancing effects of the larger Ψ. LWP is also somewhat improved compared to the simulation that does not account for SIP, however it still remains higher than the observed interquartile range.

Ice multiplication also improves the macrophysical state of the cloud in simulations with plates, as long as the cloud ice and snow particles that undergo break-up are assumed to be lightly rimed. These improvements are slightly smaller compared to the simulations with dendrites. However, prescribing a high rimed fraction for plates results in explosive multiplication, if cloud ice-to-snow autoconversion is not accounted for in the model. This is because the larger fragment generation rates are not balanced by precipitation processes and the freshly formed small fragments accumulate in the cloud ice category, continuously feeding the multiplication process until the cloud glaciates.

Since fragment generation in the parameterization by Phillips et al. (2017a,b) is constrained based on unrealistic laboratory set-ups, there is considerable uncertainty in the estimated number of fragments. The impact of the correction for sublimation effects in Vardiman's (1978) data is examined by removing the relevant correction factor. This, however, resulted in cloud glaciation in both simulations with dendrites and plates, confirming that this correction is essential to avoid an unrealistic explosive multiplication. Enhanced precipitation through activation of cloud-ice to snow autoconversion can prevent cloud dissipation in all sensitivity tests that result in explosive multiplication, except for the set-up with non-dendritic planar ice that does not include the sublimation correction factor.

ICNC enhancement in the most realistic simulations rarely exceeds a factor of 2. Yano and Phillips (2011) developed a metric for multiplication efficiency $\hat{C} = 4c_0 a\, t_f t_g$, where c_0 is the primary ice generation rate, a is the breakup rate (which is the product of the sweep-out rate and the number of fragments generated per collision), tf and tg are the timescale for fallout of large ice precipitation and time scale for conversion of small to large ice precipitation, respectively. Graupel formation occurs relatively fast in our model, thus our tg is smaller compared to the numbers adapted in previous studies (Yano and Phillips 2011; Phillips et al. 2017b; Sotiropoulou et al. 2020): 6.6 min and 7.5 min for BRPLA0.2 and BRDEN0.2 simulations, respectively. Also the number of fragments generated per snow-collision is found larger compared to warmer Arctic conditions: Sotiropoulou et al. (2020) found that maximum five fragments are generated per snow-graupel collision, while up to 13.7 (8.5) fragments are produced in the BRPLA0.2 (BRDEN0.2) simulations, respectively. While observations of Arctic clouds (Schwarzenboeck et al. 2009) also indicate that break-up of an ice particle usually produces less than 5 fragments, these estimates are only based on the examination of particles around 300 μm or roughly larger. In our simulations, mm-particles mainly contribute to ice multiplication (Fig. 5), suggesting that the estimated fragmentation number is not unreasonable. Nevertheless, substituting these parameters in the above formula yields $\hat{C}$=1.6 and $\hat{C}$=2.2 for BRDEN0.2 and BRPLA0.2 simulations, which is 4.5-5.5 times lower than the estimated efficiency found in previous studies of mesoscale convective systems (Phillips et al. 2017b) and Arctic stratocumulus clouds (Sotiropoulou et al. 2020).. While $\hat{C}$>1 implies that explosive multiplication is possible (Yano and Phillips 2011), the required time for this to happen is much longer than the time mixing-scale of the studied cloud. For this reason, such low $\hat{C}$ are associated with generally weak ICNC enhancement.

Sotiropoulou et al. (2020) found a 10-20 fold enhancement in ICNCs due to break-up compared to the available INPs and estimated $\hat{C}$=10 for Arctic clouds within the Hallet-Mossop temperature range. However their case is characterized by lower INP concentrations that do not exceed 0.1 L^{-1}, while in sensitivity tests of primary ice nucleation they showed that increasing INPs result in decreasing secondary ice production. In the present study, relatively high INP conditions are adapted. Primary ICNCs increase with time as the cloud cools through radiative cooling, reaching a maximum of 1 L^{-1} towards the end of the simulation. While primary ice formation in our set-up is likely overestimated (Fridlind et al., 2007; Wex et al., 2019), our results support the conclusions of Sotiropoulou et al. (2020) and further suggest that as primary ice nucleation becomes more and more enhanced at colder temperatures, ice multiplication from ice-ice collisions will likely become less significant. It is interesting that while laboratory experiments from Takahashi et al. (1995), based on collisions of two hailstones, suggest increasing ice multiplication with decreasing temperature from -3°C to -15°C, our

findings indicate that this might not happen in the real atmosphere due to the increasing availability of INPs.

Finally, the possibility that ice multiplication is still underestimated in our simulations cannot be excluded, since MIMICA predicts that only 10-12% of the simulated ice particles in BRDEN0.2 and BRPLA0.2 simulations contribute to ice multiplication through break-up. Schwarzenboeck et al (2009) found indications of fragmentation in 55% of the examined ice particles, although natural fragmentation could only be confirmed for 18%, while their sample was characterized by relatively small sizes. Moreover, while processes like rime-splintering and drop-shattering are clearly ineffective in the examined conditions, the contribution from other SIP mechanisms has not been investigated, e.g. blowing snow and fragmentation of sublimating particles (Field et al. 2017). Sublimation of cloud ice particles can occur if cloud conditions become subsaturated with respect to ice; however a preliminary inspection of the domain-averaged supersaturation profiles did not reveal any such evidence. Furthermore, blowing snow is associated with relatively high wind speeds (Gossart et al, 2017), while during the examined ASCOS case the maximum wind speed never exceeded 5.2 m s^{-2} in the boundary layer.

6. Conclusions

In this study, ice multiplication from ice-ice collisions is implemented in the MIMICA LES, following Phillips et al. (2017a,b), to investigate the role of this process for ice-liquid partitioning in a summertime Arctic low-level cloud deck observed during ASCOS. The sensitivity of the simulated results to the prescribed ice habit and rimed fraction is examined. The impact of changes in ice content distribution among the three ice categories is also investigated by accounting for cloud ice-to-snow autoconversion and thus enhancing snow. The last set of sensitivity tests concerns the sublimation correction factor adapted in the parameterization, which is a highly uncertain parameter. Our findings can be summarized as follows:

- For the simulated temperature range (-12.5 to -7 ^{o}C), ice multiplication from collisional break-up is generally weak, enhancing ICNCs by on average no more than a factor of 1.5-2 in the simulations that are most consistent with observations. Increases in ICNCs due to break-up are compensated by increased precipitation and sublimation in the sub-cloud layer. Simulation set-ups that produce a 10-fold ICNC enhancement result in cloud dissipation.
- While activation of break-up can substantially improve the agreement between modeled and observed cloud ice content, the impact on cloud liquid is weaker. Ice multiplication can decrease the

505   median LWP by 25-35 g m^{-2}, resulting in better agreement with observations. Yet cloud liquid
        content remains overestimated in the model.

- Ice multiplication from break-up of dendrites is not very sensitive to assumptions regarding the rimed
    fraction. Break-up of lightly rimed non-dendritic planar ice also produces similar cloud water
    properties as in the simulations with dendrites. In contrast, break-up of highly rimed plates can lead
510   to cloud dissipation, if cloud ice-to-snow autoconversion is not accounted for in the microphysics
    scheme. Activating cloud ice-to-snow autoconversion enhances the precipitation sink, which
    prevents accumulation of cloud ice particles, excessive multiplication and cloud dissipation.

- Removing the correction factor for sublimation effects from the Phillips et al. (2017a,b)
    parameterization results in cloud glaciation, independently of the assumed ice habit. Activation of
515   cloud ice-to-snow autoconversion can prevent explosive multiplication in this set-up only for
    simulations with dendrites. The large sensitivity of the results suggest that this factor is likely the
    most important source of uncertainty in the representation of break-up, especially for non-dendritic
    planar ice particles.

520   The generally low sensitivity of our results to assumptions regarding ice habit and rimed fraction
indicate that the lack of an explicit prediction of these properties in climate models is not detrimental for
the representation of ice multiplication effects due to break-up in Arctic clouds. The sensitivity,
however, is in some set-ups influenced by the way snow formation is treated, since snow precipitation
can prevent continuous accumulation of ice particles within the cloud layer. Cloud ice-to-snow
525   autoconversion appears to be a key process to sustain the balance between ice sources and sinks and this
process is usually considered in most climate model bulk microphysics schemes (e.g. Murakami 1990;
Morrison and Gettelman 2008). Finally, we acknowledge that the weak influence of the rimed fraction is
likely limited for conditions characterized by weak multiplication efficiency ($\hat{C} \approx 2$) and thus weak ICNC
enhancement, as those examined here. Future model development plans include the treatment of rimed
530   fraction as a prognostic variable; this is likely important for the study of collisional break-up effects in
more convective clouds.

Code and data availability: ASCOS data are available at https://bolin.su.se/data/ascos/ . The modified
LES code is available upon request.

535

Competing interests: The authors declare that they have no conflict of interest.

Author contribution: GS implemented the break-up parameterization in the LES, performed the

simulations, analyzed the results and led manuscript writing. LI implemented the primary ice nucleation scheme. All authors contributed to the scientific interpretation, discussion and writing of the manuscript.

Acknowledgements: GS, AN and AE acknowledge support from the project IC-IRIM (project ID 2018-01760) funded by the Swedish Research Council for Sustainable Development (FORMAS) and the project FORCeS funded from Horizon H2020-EU.3.5.1. (project ID 821205). LI supported by Chalmers Gender Initiative for Excellence (Genie). The authors are also grateful to ASCOS scientific crew for the observational datasets used in this study and to two anonymous reviewers for very constructive comments. The computations were enabled by resources provided by the Swedish National Infrastructure for Computing (SNIC) at the National Supercomputer Centre (NSC) partially funded by the Swedish Research Council through grant agreement no. 2016-07213.

APPENDIX A: PRIMARY ICE PRODUCTION

The immersion freezing parameterization is based on the concept of ice nucleation active site density. The formulation of Niemand et al. (2012) is used, adapted for microline dust particles (Ickes et al., 2017). It is utilized here as the only primary ice production mechanism. In this scheme, the number of nucleated ice particles (N_{INP}, m^{-3}) is given as function of N_{CCN} and temperature T (°C) :

$$N_{INP} = X N_{CCN}\left(1 - e^{-4\pi r^2 n_s}\right),$$

where $n_s = e^{-aT+b}$. X is the percentage of N_{CCN} (m^{-3}) that acts as efficient INP, e.g. 50%, 10%, 5% (see Text S1 in Supporting Information) and n_s (m^{-2}) the ice nucleation active site density of the INP species assumed (here microcline). $r = 46.5 \cdot 10^{-9}$ m is the mean radius of the accumulation aerosol mode measured during the examined ASCOS case (Ickes et al., in prep.). The temperature dependency is determined by the coefficients $\alpha = 0.73$°C^{-1} and $b = 9.63$.

APPENDIX B: ICE MUTIPLICATION FROM ICE-ICE COLLISIONS

A bulk description of the collisional break-up process is applied, which is based on existing descrpriptions of the interactions between the three ice particle types (cloud ice, snow and graupel) and within the same category (Wang and Chang 1993). Ice multiplication is allowed after cloud ice-cloud ice cloud ice-snow, cloud ice-graupel, graupel-snow, snow-snow and graupel-graupel collisions. For collisions between different ice types, the rate of number ($P_{n12} \wedge mass(P_{m12})$concentration of particle 1 that is collected by particle 2 is given:

$$P_{n12} = \frac{\pi}{4}\rho E_{col} N_1 N_2 \quad (1)$$

$$P_{q12} = \frac{\pi}{4}\rho E_{12}Q_1 N_2 \quad (2)$$

where subsrcript 'n' and 'm' denote number- and mass- weighted parameters, respectively. N and Q refer to number and mass concentration of the particle, while D and v represent its diameter and terminal velocity. a is the shape parameter of the size distribution for each particle, set to 2 for cloud ice (independently of the ice habit, 1 for snow and 0 for graupel, while b_v is a coefficient in the fallspeed-diameter relationship (see Section 3.3.1). E_{col} is the collection efficiency, given as a function of temperature (K): $E_{col} = exp[0.09(T\text{-}273.15)]$. For self-collection, thus collisions between same ice types, the above equations take the form:

$$P_{n11} = \frac{\pi}{2}\rho E_{col}N_1 N_1 \quad (3)$$

$$P_{q11} = \frac{\pi}{2}\rho E_{col}N_1 Q_1 \quad (4).$$

The above equations are further used to determine collisions that result in ice multiplication, by replacing the collection efficiency with the term $E^*=1\text{-}E_{col}$. This means that the collisions that do not result in aggregation are those that contribute to SIP. Since aggregation after cloud-ice-graupel and graupel-graupel collisions does not occur, we assume that 100% of these collisions result in multiplication: $E^*=1$.

The Phillips et al. (2017a) parameterization allows for varying treatment of F_{BR} depending on the ice crystal type and habit:

$$F_{BR} = \alpha A \left(1 - exp\left\{-\left[\frac{CK_o}{\alpha A}\right]^\gamma\right\}\right) \quad (5)$$

$K_o = \frac{m_1 m_2}{m_1+m_2}\left(\Delta u_{n_{12}}\right)^2$ represents collisional kinetic energy and $a = \pi D^2$, where D (in meters) is the size of the smaller ice particle which undergoes fracturing and α is its surface area. m_1, m_2 are the masses of the colliding particles and Δu_{n12} is the difference in their terminal velocities. A correction is further

applied in Δu_{n12} to account for underestimates when $u_{n1} \approx u_{n2}$, following Mizuno et al. (1990) and Reisner et al. (1998):

$$\left|\Delta u_{n_{12}}\right| = ((1.7u_{n1} - u_{n2})^2 + 0.3u_{n1}u_{n2})^{1/2}$$

A represents the number density of the breakable asperities in the region of contact. C is the asperity-

fragility coefficient, which is a function of a correction term (ψ) for the effects of sublimation based on the field observations by Vardiman (1978). Exponent γ is a function of rimed fraction for collisions that include cloud ice and snow. Particularly, for non-dendritic planar ice or snow, with rimed fraction $\Psi <$ 0.5, that undergoes fracturing after collisions with other ice particles:

$$A = 1.58 \cdot 10^7 (1 + 100\Psi^2)\left(1 + \frac{1.33 \cdot 10^{-4}}{D^{1.5}}\right) \ (6),$$

$$C = 7.08 \times 10^6 \psi$$

$$\psi = 3.5 \times 10^{-3}$$

$$\gamma = 0.5 - 0.25\Psi$$

For fragmentation of dendrites, A and C are somewhat different :

$$A = 1.41 \cdot 10^6 (1 + 100\Psi^2)\left(1 + \frac{3.98 \cdot 10^{-5}}{D^{1.5}}\right) \ (7),$$

$$C = 3.09 \times 10^6 \psi$$

$$\psi = 3.5 \times 10^{-3}$$

$$\gamma = 0.5 - 0.25\Psi$$

For graupel-graupel collisions, an explicit temperature dependency is included in the equation, while γ is contant:

$$A = \frac{a_o}{3} + \max\left(\frac{2a_o}{3} - \frac{a_o}{9}|T - 258|, 0\right) \ (8),$$

$$a_o = 3.78 \cdot 10^4 \cdot \left(1 + \frac{0.0079}{D^{1.5}}\right)$$

$$C = 6.3 \times 10^6$$

$$\psi = 3.5 \times 10^{-3}$$

$$\gamma = 0.3$$

The parameterization was developed based on particles with diameters 500 μm $< D <$ 5 mm, however Phillips et al. (2017a) suggest that it can be used for particle sizes outside the recommended range as long as the input variables to the scheme are set to the nearest limit of the range. Moreover, an upper limit for the number of fragments produced per collision is imposed, set to $F_{BR_{max}} = 100$ (Phillips et al., 2017a), for all collision types. The production rate of fragments is estimated using Eq. (1) or (3) and one of the proposed formulations for F_{BR} above, e.g. $P_{BR12}P_{n12}F_{BR}$. Whenever mass transfer also occurs, e.g. if assume that fragments ejected from snow-gruapel collisions are added to the cloud ice category, we assume that this is only 0.1% of colliding mass (Eq. (2) or (4)) that undergoes break-up (Phillips et al. 2017a).

APPENDIX C: CLOUD ICE - TO - SNOW AUTOCONVERSION

For cloud ice-to-snow autoconversion, we use the formula adapted in Wang and Chang (1993) for cloud
ice-to-graupel and graupel-to-hail autoconversion:

$$P_{q\text{auto}} = Q_i e^{D_c \lambda} \left\{ 1 + D_c \lambda \left[1 + D_c \lambda \left(0.5 + \frac{D_c \lambda}{6} \right) \right] \right\}$$

$$P_{n\text{auto}} = N_i e^{D_c \lambda} (1 + D_c \lambda)$$

where $\lambda = \left[\frac{A_m \Gamma(\alpha + b_m + 1) N_i}{\Gamma(\alpha + 1) Q_i} \right]^{1/b_m}$

and D_c is the critical diameter that separates the two ice cateogries. N_i and Q_i are the number and mass
cloud ice concentrations, respectively.

References

Andronache, C.: Characterization of Mixed-Phase Clouds: Contributions From the Field Campaigns and
Ground Based Networks, in: Mixed-Phase Clouds: Observations and Modeling, edited by: Andronache,
C., pp. 97–120, Elsevier, the Netherlands, UK, USA, https://doi.org/10.1016/B978-0-12-810549-
8.00005-2, 2017.

Atkinson, J. D., Murray, B. J., Woodhouse, M. T., Whale, T. F., Baustian, K. J., Carslaw, K. S., Dobbie,
S., O'Sullivan, D., and Malkin, T. L.: The importance of feldspar for ice nucleation by mineral dust in
mixed-phase clouds, Nature, 498, 355–358, https://doi.org/10.1038/nature12278, 2013.

Bigg, E. K. and Leck, C.: Cloud-active particles over the central Arctic Ocean, J. Geophys. Res., 106,
32155–32166, doi:10.1029/1999JD901152, 2001.

Burt, M. A., Randall, D. A., and Branson, M. D.: Dark warming. Journal Climate, 29, 705–719, 2015

Cao, Y., Liang, S., Chen, X., He, T., Wang, D., and Cheng, X.: Enhanced wintertime greenhouse effect
reinforcing Arctic amplification and initial sea-ice melting. Scientific Reports, 7, 8462, 2017

Choularton, T.W., Griggs, D.J. , Humood, B.Y., and Latham, J. : Laboratory studies of riming, and its
relation to ice splinter production. Quart. J. Roy. Meteor. Soc., 106, 367–374,
doi:https://doi.org/10.1002/qj.49710644809., 1980

Connolly, P. J., Möhler, O., Field, P. R., Saathoff, H., Burgess, R., Choularton, T., and Gallagher, M.: Studies of heterogeneous freezing by three different desert dust samples, Atmos. Chem. Phys., 9, 2805–2824, https://doi.org/10.5194/acp-9-2805-2009, 2009.

765 Cronin, T. W., and Tziperman, E. : Low clouds suppress Arctic air formation and amplify high-latitude continental winter warming. Proceedings of the National Academy of Sciences, 112, 11,490– 11,495, 2015

Durran, D.R.: Numerical Methods for Fluid Dynamics, Texts Appl. Math., 2nd ed., Springer, Berlin-770 Heidelberg, Germany, 2010.

Field, P., Lawson, P., Brown, G., Lloyd, C., Westbrook, D., Moisseev, A., Miltenberger, A., Nenes, A., Blyth, A., Choularton, T., Connolly, P., Bühl, J., Crosier, J., Cui, Z., Dearden, C., DeMott, P., Flossmann, A., Heymsfield, A., Huang, Y., Kalesse, H., Kanji, Z., Korolev, A., Kirchgaessner, A., 775 Lasher-Trapp, S., Leisner, T., McFarquhar, G., Phillips, V., Stith, J., and Sullivan, S.: Chapter 7: Secondary ice production - current state of the science and recommendations for the future, Meteor. Monogr., doi:10.1175/AMSMONOGRAPHS-D-16-0014.1, 2017.

Fridlind, A. M., Ackerman, A. S., McFarquhar, G., Zhang, G., Poellot, M. R., DeMott, P. J., Prenni, A. 780 J., and Heymsfield, A. J.: Ice properties of single-layer stratocumulus during the Mixed-Phase Arctic Cloud Experiment: 2. Model results., J. Geophys. Res., 112, D24202, https://doi.org/10.1029/2007JD008646, 2007.

Fridlind, A.M., van Diedenhoven, B., Ackerman, A.S., Avramov, A., Mrowiec, A., Morrison, H., 785 Zuidema, P., and Shupe M.D.: A FIRE-ACE/SHEBA Case Study of Mixed-Phase Arctic Boundary Layer Clouds: Entrainment Rate Limitations on Rapid Primary Ice Nucleation Processes. J. Atmos. Sci., 69, 365–389, https://doi.org/10.1175/JAS-D-11-052.1, 2012

Fridlind, A. M., and Ackerman, A.S. : Simulations of Arctic Mixed-Phase Boundary Layer Clouds: 790 Advances in Understanding and Outstanding Questions, Mixed-Phase Clouds: Observations and Modeling, 153-183, doi:10.1016/B978-0-12-810549-8.00007-6, 2019

Fu, Q, and Liou K.N: On the Correlated k-Distribution Method for Radiative Transfer in Nonhomogeneous Atmospheres, J. Atmos., 49(22): 2139–2156, doi: 10.1007/s00382-016-3040-8, 1992

795   Fu, S., Deng, X., Shupe, M.D., and Huiwen X.: A modelling study of the continuous ice formation in an autumnal Arctic mixed-phase cloud case, Atmos. Res., 228, 77-85, https://doi.org/10.1016/j.atmosres.2019.05.021, 2019

800   Gayet, J.-F., Treffeisen, R., Helbig, A., Bareiss, J., Matsuki, A., Herber, A., and Schwarzenboeck, A.: On the onset of the ice phase in boundary layer Arctic clouds, J. Geophys. Res., 114, D19201, doi:10.1029/2008JD011348, 2009

Gossart, A., Souverijns, N., Gorodetskaya, I. V., Lhermitte, S., Lenaerts, J. T. M., Schween, J. H.,
805   Mangold, A., Laffineur, Q., and van Lipzig, N. P. M.: Blowing snow detection from ground-based ceilometers: application to East Antarctica, The Cryosphere, 11, 2755–2772, https://doi.org/10.5194/tc-11-2755-2017, 2017.

Hallett, J. and Mossop, S. C.: Production of secondary ice particles during the riming process, Nature,
810   249, 26–28, doi:10.1038/249026a0, 1974.

Hong, S., J. Dudhia, and S. Chen: A Revised Approach to Ice Microphysical Processes for the Bulk Parameterization of Clouds and Precipitation. Mon. Wea. Rev., 132, 103–120, https://doi.org/10.1175/1520-0493(2004)132<0103:ARATIM>2.0.CO;2, 2004
815

Jensen A. A., Harrigton J. Y., Morrison H. and J.A. Milbrandt: Prediciting Ice Shape Evolution in a Bulk Microphysics Model, J. Atmos. Sci., 74(6), 2081-2104, https://doi.org/10.1175/JAS-D-16-0350.1, 2017

Ickes, L., Welti, A., and Lohmann, U.: Classical nucleation theory of immersion freezing: sensitivity of
820   contact angle schemes to thermodynamic and kinetic parameters, Atmos. Chem. Phys., 17, 1713–1739, https://doi.org/10.5194/acp-17-1713-2017, 2017.

Ickes, L. and Ekman, A. : What is triggering freezing in warm Arctic mixed-phase clouds? A modelling study with MIMICA LES. in preparation, 2021
825

Igel, A. L., Ekman, A. M. L., Leck, C., Savre, J., Tjernström, M., and Sedlar, J.: The free troposphere as a potential source of Arctic boundary layer aerosol particles. Geophys. Res. Let.s, 44, 7053–706, doi:10.1002/2017GL073808, 2017

330   Kay, J. E., L'Ecuyer, T., Chepfer, H., Loeb, N., Morrison, A., & Cesana, G: Recent advances in Arctic cloud and climate research. Current Climate Change Reports, 2, 159–169, 2016

Khvorostyanov, V.I., and Curry J.A: Terminal Velocities of Droplets and Crystals: Power Laws with Continuous Parameters over the Size Spectrum. *J. Atmos. Sci.,* 59,1872 1884,
335   https://doi.org/10.1175/1520-0469(2002)059<1872:TVODAC>2.0.CO;2, 2002

Khvorostyanov, V. I., and Curry, J. A.: Aerosol size spectra and CCN activity spectra: Reconciling the lognormal, algebraic, and power laws, J. Geophys. Res., 111, D12202, doi:10.1029/2005JD006532, 2006
340

Korolev, A., McFarquhar, G., Field, P.R., Franklin, C., Lawson, P., Wang, Z., Williams, E., Abel, S.J., Axisa, D., Borrmann, S., Crosier, J., Fugal, J., Krämer, M., Lohmann, U., Schlenczek, O., Schnaiter, M., and Wendisch, M.: Mixed-Phase Clouds: Progress and Challenges. Meteorological Monographs, 58, 5.1–5.50, https://doi.org/10.1175/AMSMONOGRAPHS-D-17-0001.1, 2017
345

Lauber, A., Kiselev, A., Pander, T., Handmann, P., and Leisner, T.: Secondary ice formation during freezing of levitated droplets, J. Atmos. Sci., 75, 2815–2826, https://doi.org/10.1175/JAS-D-18-0052.1, 2018.

Leck, C., Norman, M., Bigg, E. K., and Hillamo, R.: Chemi- cal composition and sources of the high
350   Arctic aerosol rele- vant for fog and cloud formation, J. Geophys. Res., 107, 4135, doi:10.1029/2001JD001463, 2002.

Lilly, D.K.: A proposed modification to the Germano subgrid-scale closure method, Phys. Fluids, 4: 633–635, doi:10.1063/1.858280, 1992.

355   Loewe, K., Ekman, A. M. L., Paukert, M., Sedlar, J., Tjernström, M., and Hoose, C.: Modelling micro- and macrophysical contributors to the dissipation of an Arctic mixed-phase cloud during the Arctic Summer Cloud Ocean Study (ASCOS), Atmos. Chem. Phys., 17, 6693–6704, https://doi.org/10.5194/acp-17-6693-2017, 2017.

360   Lloyd, G., Choularton, T. W., Bower, K. N., Crosier, J., Jones, H., Dorsey, J. R., Gallagher, M. W., Connolly, P., Kirchgaessner, A. C. R., and Lachlan-Cope, T.: Observations and comparisons of cloud

microphysical properties in spring and summertime Arctic stratocumulus clouds during the ACCACIA campaign, Atmos. Chem. Phys., 15, 3719–3737, https://doi.org/10.5194/acp-15-3719-2015, 2015.

Moore, R. H., Bahreini, R., Brock, C. A., Froyd, K. D., Cozic, J., Holloway, J. S., Middlebrook, A. M., Murphy, D. M., and Nenes, A.: Hygroscopicity and composition of Alaskan Arctic CCN during April 2008, Atmos. Chem. Phys., 11, 11807–11825, https://doi.org/10.5194/acp-11-11807-2011, 2011

Moran, K. P., Martner, B. E., Post, M. J., Kropfli, R. A., Welsh, D. C., and Widener, K. B.: An unattended cloud-profiling radar for use in climate research, B. Am. Meteorol. Soc., 79, 443–455, doi:10.1175/1520-0477(1998)079<0443:AUCPRF>2.0.CO;2, 1998.

Morrison, H. and A. Gettelman, 2008: A New Two-Moment Bulk Stratiform Cloud Microphysics Scheme in the Community Atmosphere Model, Version 3 (CAM3). Part I: Description and Numerical Tests. J. Climate, 21, 3642–3659, https://doi.org/10.1175/2008JCLI2105.1

Morrison, H. and J.A. Milbrandt: Parameterization of cloud microphysics based on the prediction of bulk ice particle properties. Part I: Scheme description and idealized tests. *J. Atmos. Sci.*, *72*, 287-311. doi:10.1175/JAS-D-14-0065.1, 2015

Mioche, G., Jourdan, O., Delanoë, J., Gourbeyre, C., Febvre, G., Dupuy, R., Monier, M., Szczap, F., Schwarzenboeck, A., and Gayet, J.-F.: Vertical distribution of microphysical properties of Arctic springtime low-level mixed-phase clouds over the Greenland and Norwegian seas, Atmos. Chem. Phys., 17, 12845–12869, https://doi.org/10.5194/acp-17-12845-2017, 2017.

Murakami, M.: Numerical modeling of dynamical and microphysical evolution of an isolated convective cloud: The 19 July 1981 CCOPE cloud. J. Meteor. Soc. Japan, 68, 107-128, 1990

Mizuno, H.: Parameterization if the accretion process between different precipitation elements. J. Meteor. Soc. Japan, 57, 273-281, 1990

Morrison, H., Curry, J.A., and Khvorostyanov, V.I.: A New Double-Moment Microphysics Parameterization for Application in Cloud and Climate Models. Part I: Description, Atmos. Sci.*, 62,* 3683-3704 62, 2005

Niemand, M., O. Möhler, B. Vogel, H. Vogel, C. Hoose, P. Connolly, H. Klein, H. Bingemer, P. DeMott, J. Skrotzki, and Leisner, T.: A Particle-Surface-Area-Based Parameterization of Immersion

Freezing on Desert Dust Particles. J. Atmos. Sci., 69, 3077–3092, https://doi.org/10.1175/JAS-D-11-0249.1 , 2012

Phillips, V. T. J., Yano, J.-I., and Khain, A.: Ice multiplication by breakup in ice-ice collisions. Part I: Theoretical formulation, J. Atmos. Sci., 74, 1705–1719, https://doi.org/10.1175/JAS-D-16-0224.1, 2017a.

Phillips, V.T., Yano, , J.-I., Formenton, M., Ilotoviz, E., Kanawade, V., Kudzotsa, I., Sun, J., Bansemer, A., Detwiler, A.G., Khain, A., and Tessendorf, S.A.: Ice Multiplication by Breakup in Ice–Ice Collisions. Part II: Numerical Simulations. J. Atmos. Sci., 74, 2789–2811, https://doi.org/10.1175/JAS-D-16-0223.1, 2017b.

Phillips, V.T., S. Patade, J. Gutierrez, and A. Bansemer, A.: Secondary Ice Production by Fragmentation of Freezing Drops: Formulation and Theory. J. Atmos. Sci., 75, 3031–3070, https://doi.org/10.1175/JAS-D-17-0190.1, 2018

Pruppacher, H.R., and Klett, J.D. : Microphysics of Clouds and Precipitation. 2nd Edition, Kluwer Academic, Dordrecht, 954 p., 1997

Rangno, A. L., and Hobbs, P. V.: Ice particles in stratiform clouds in the Arctic and possible mechanisms for the production of high ice concentrations, J. Geophys. Res., 106, 15,065–15,075, doi:10.1029/2000JD900286, 2001.

Reisner, J., Rasmussen, R. M., and Bruintjes, R. T.: Explicit forecasting of supercooled liquid water in winter storms using the MM5 mesoscale model, Quart. J. Roy. Meteor. Soc, 124(548), 1071{1107}, doi: 10.1002/qj.49712454804, 1998.

Roberts, G. C. and Nenes, A. A.: continuous-flow stream- wise thermal-gradient CCN chamber for atmospheric measurements, Aerosol Sci. Technol., 39, 206–221, doi:10.1080/027868290913988, 2005.

Savre, J, Ekman, AML, and Svensson, G.: Technical note: Introduction to MIMICA, a large-eddy simulation solver for cloudy planetary boundary layers, J. Adv. Model. Earth Syst., 6, doi:10.1002/2013MS000292, 2014.

925 Schwarzenboeck, A., Shcherbakov,V., Lefevre, R., Gayet, J.-F., Duroure, C., and Pointin, Y.: Evidence for stellar-crystal fragmentation in Arctic clouds,Atmos. Res.,92, 220–228, doi:10.1016/j.atmosres.2008.10.002, 2009

Sedlar, J., Shupe, M. D., and Tjernström, M.: On the relationship between thermodynamic structure, 930 cloud top, and climate significance in the Arctic, J. Climate, 25, 2374–2393, doi:10.1175/JCLI-D-11-00186.1, 2012.

Seifert, A., and Beheng. K. D: A double-moment parameterization for simulating auto conversion, accretion and self collection, Atmos. Res., 59–60: 265–281, doi:10.1016/S0169-8095(01)00126-0, 2001. 935

Shupe, M. D., Uttal, T., and Matrosov, S. Y.: Arctic cloud micro- physics retrievals from surface-based remote sensors at SHEBA, J. Appl. Meteor. Clim., 44, 1544–1562, doi:10.1175/JAM2297.1, 2005.

Sotiropoulou, G, Sedlar, J, Tjernström, M, Shupe, MD, Brooks, IM, Persson, POG:The thermodynamic structure of summer Arctic stratocumulus and the dynamic coupling to the surface. Atmos. Chem. Phys., 940 14, 12573 – 12592, doi: 10.5194/acp-14-12573-2014, 2014.

Sotiropoulou, G., Sullivan, S., Savre, J., Lloyd, G., Lachlan-Cope, T., Ekman, A. M. L., and Nenes, A.: The impact of Secondary Ice Production on Arctic Stratocumulus, Atmos. Chem. Phys., 20, 1301–1316, https://doi.org/10.5194/acp-2019-804, 2020a.

Sotiropoulou G., Vignon E., Young G., Morrison H., O'Shea S.J., Lachlan-Cope T., Berne A., Nenes A.: 945 Secondary ice production in Antarctic mixed-phase clouds: an underappreciated process in atmospheric models, Atmos. Chem. Phys. Discuss., https://doi.org/10.5194/acp-2020-328, in review, 2020b.

Stevens, R. G., Loewe, K., Dearden, C., Dimitrelos, A., Possner, A., Eirund, G. K., Raatikainen, T., Hill, A. A., Shipway, B. J., Wilkinson, J., Romakkaniemi, S., Tonttila, J., Laaksonen, A., Korhonen, H., Connolly, P., Lohmann, U., Hoose, C., Ekman, A. M. L., Carslaw, K. S., and Field, P. R.: A model 950 intercomparison of CCN-limited tenuous clouds in the high Arctic, Atmos. Chem. Phys., 18, 11041–11071, https://doi.org/10.5194/acp-18-11041-2018, 2018.

Stocker, T.F., D. Qin, G.-K. Plattner, L.V. Alexander, S.K. Allen, N.L. Bindoff, F.-M. Bréon, J.A. Church, U. Cubasch, S. Emori, P. Forster, P. Friedlingstein, N. Gillett, J.M. Gregory, D.L. Hartmann, E. 955 Jansen, B. Kirtman, R. Knutti, K. Krishna Kumar, P. Lemke, J. Marotzke, V. Masson-Delmotte, G.A. Meehl, I.I. Mokhov, S. Piao, V. Ramaswamy, D. Randall, M. Rhein, M. Rojas, C. Sabine, D. Shindell,

L.D. Talley, D.G. Vaughan, and S.-P. Xie: Technical summary. In Climate Change 2013: The Physical Science Basis. Contribution of Working Group I to the Fifth Assessment Report of the Intergovernmental Panel on Climate Change. T.F. Stocker, D. Qin, G.-K. Plattner, M. Tignor, S.K. Allen, J. Doschung, A. Nauels, Y. Xia, V. Bex, and P.M. Midgley, Eds. Cambridge University Press, pp. 33-115, doi:10.1017/CBO9781107415324.005, 2013

Takahashi, T., Nagao, Y., and Kushiyama, Y.: Possible high ice particle production during graupel-graupel collisions, J. Atmos. Sci., 52, 4523–4527, doi:10.1175/1520-0469, 1995.

Tan, I., and Storelvmo, T. : Evidence of strong contributions from mixed-phase clouds to Arctic climate change. Geophysical Research Letters, 46, 2894-2902. https://doi.org/10.1029/2018GL081871, 2019

Taylor, P. C., Boeke, R. C., Li, Y., and Thompson, D. W. J.: Arctic cloud annual cycle biases in climate models, Atmos. Chem. Phys., 19, 8759–8782, https://doi.org/10.5194/acp-19-8759-2019, 2019.

Tjernström, M., Birch, C. E., Brooks, I. M., Shupe, M. D., Pers- son, P. O. G., Sedlar, J., Mauritsen, T., Leck, C., Paatero, J., Szczodrak, M., and Wheeler, C. R.: Meteorological conditions in the central Arctic summer during the Arctic Summer Cloud Ocean Study (ASCOS), Atmos. Chem. Phys., 12, 6863–6889, doi:10.5194/acp-12-6863-2012, 2012.

Tjernström, M., Leck, C., Birch, C. E., Bottenheim, J. W., Brooks, B. J., Brooks, I. M., Bäcklin, L., Chang, R. Y.-W., de Leeuw, G., Di Liberto, L., de la Rosa, S., Granath, E., Graus, M., Hansel, A., Heintzenberg, J., Held, A., Hind, A., Johnston, P., Knulst, J., Martin, M., Matrai, P. A., Mauritsen, T., Müller, M., Norris, S. J., Orellana, M. V., Orsini, D. A., Paatero, J., Persson, P. O. G., Gao, Q., Rauschenberg, C., Ristovski, Z., Sedlar, J., Shupe, M. D., Sierau, B., Sirevaag, A., Sjogren, S., Stetzer, O., Swietlicki, E., Szczodrak, M., Vaattovaara, P., Wahlberg, N., Westberg, M., and Wheeler, C. R.: The Arctic Summer Cloud Ocean Study (AS- COS): overview and experimental design, Atmos. Chem. Phys., 14, 2823–2869, doi:10.5194/acp-14-2823-2014, 2014.

Vardiman, L.: The generation of secondary ice particles in clouds by crystal-crystal collision, J. Atmos. Sci., 35, 2168–2180, doi:10.1175/1520-0469, 1978.

Wang, C., and J. Chang, J.: A three-dimensional numerical model of cloud dynamics, microphysics, and chemistry. 1: Concepts and formulation, J. Geophys. Res., 98, 16,787–16,798, doi:10.1029/92JD01393, 1993.

990 Williams, P.D.: The RAW filter: An improvement to the Robert-Asselin filter in semi-implicit integrations, Mon. Weather Rev., 139: 1996–2007, doi:10.1175/2010 MWR3601.1, 2010

Yano, J.-I. and Phillips, V. T. J.: Ice-ice collisions: an ice multiplication process in atmospheric clouds, J. Atmos. Sci., 68, 322–333, doi:10.1175/2010JAS3607.1, 2011.

995

Yano, J.-I., Phillips, V. T. J., and Kanawade, V.: Explosive ice multiplication by mechanical break-up in-ice-ice collisions: a dynamical system-based study, Q. J. Roy. Meteor. Soc., 142, 867–879, https://doi.org/10.1002/qj.2687, 2015.

000 Young, G., Lachlan-Cope, T., O'Shea, S. J., Dearden, C., Listowski, C., Bower, K. N., Choularton T.W., and Gallagher M.W.: Radiative effects of secondary ice enhancement in coastal Antarctic clouds. Geophys. Res. Let. , 46 , 23122321, https://doi.org/10.1029/2018GL080551, 2019

Westwater, E. R., Han, Y., Shupe, M. D., and Matrosov, S. Y.: Analysis of integrated cloud liquid and
005 precipitable water va- por retrievals from microwave radiometers during SHEBA, J. Geophys. Res., 106, 32019–32030, doi:10.1029/2000JD000055, 2001.

Wex, H., Huang, L., Zhang, W., Hung, H., Traversi, R., Becagli, S., Sheesley, R. J., Moffett, C. E., Barrett, T. E., Bossi, R., Skov, H., Hünerbein, A., Lubitz, J., Löffler, M., Linke, O., Hartmann, M., Herenz, P., and Stratmann, F.: Annual variability of ice-nucleating particle concentrations at different
010 Arctic locations, Atmos. Chem. Phys., 19, 5293-5311, https://doi.org/10.5194/acp-19-5293-2019, 2019.

Zhao, X., Liu, X., Phillips, V. T. J., and Patade, S.: Impacts of secondary ice production on Arctic mixed-phase clouds based on ARM observations and CAM6 single-column model simulations, Atmos. Chem. Phys., 21, 5685–5703, https://doi.org/10.5194/acp-21-5685-2021, 2021.

015

020

Tables:

Table 1: Characteristic parameters in the mass-diameter ($m = a_m D^{bm}$) and fallspeed-diameter ($v = a_v D^{bv}$) relationships (see Section 3.3.1).

Ice type	a_m	b_m	a_v	b_v
dendritic cloud ice	0.0233	2.29	5.02	0.48
planar cloud ice	1.43	2.79	17	0.62
snow	0.04	2	11.72	0.41
graupel	65	3	19.5	0.37

Table 2: List of sensitivity simulations (see Section 3.3).

Simulation	Breakup process	Ice Habit	Rimed Fraction	Other modifications
CNTRLDEN	off	dendrite	–	none
CNTRLPLA	off	plate	–	none
BRDEN0.1	on	dendrite	0.1	none
BRDEN0.2	on	dendrite	0.2	none
BRDEN0.4	on	dendrite	0.4	none
BRPLA0.1	on	plate	0.1	none
BRPLA0.2	on	plate	0.2	none
BRPLA0.4	on	plate	0.4	none
BRDEN0.4auto	on	dendrite	0.4	active cloud ice-to-snow autoconversion
BRPLA0.2auto	on	plate	0.2	active cloud ice-to-snow autoconversion
BRPLA0.4auto	on	plate	0.4	active cloud ice to snow autoconversion
BRDEN0.4auto	on	dendrite	0.4	active cloud ice-to-snow autoconversion
BRPLA0.2auto	on	plate	0.2	active cloud ice-to-snow autoconversion
BRDENsub	on	dendrite	0.2	no correction for sublimation effects
BRPLAsub	on	plate	0.2	no correction for sublimation effects
BRDENsubauto	on	dendrite	0.2	no correction for sublimation & cloud ice-to-snow autoconversion
BRPLAsubauto	on	plate	0.2	no correction for sublimation & cloud ice-to-snow autoconversion

 Table 3: 25th, 50th (median) and 75th percentile of LWP and IWP timeseries. All variables are in g m^{-2}.

Simulation	25th perc. LWP	Median LWP	75th perc. LWP	25th perc. IWP	Median IWP	75th perc. IWP
ASCOS	52.7	73.8	89.3	4.2	7.0	11.4
CNTRLDEN	132.4	141.8	146.2	1.3	2.2	3.2
CNTRLPLA	130.9	139.1	145.7	1.2	1.8	2.7
BRDEN0.1	99.7	106.5	114.4	3.6	5.8	8.2
BRDEN0.2	107.4	109.1	118.0	4.4	6.0	7.2
BRDEN0.4	99.3	107.2	118.9	3.6	5.4	7.7
BRPLA0.1	110.0	116.6	128.8	2.4	4.2	6.9
BRPLA0.2	110.0	119.6	128.9	2.4	4.8	6.5
BRPLA0.4	0.76	39.7	99.3	0.0	0.0	1.6
CNTRDENauto	127.7	139.5	147.3	1.3	2.2	4.0
BRDEN0.2auto	100.9	109.1	116.1	3.9	5.8	7.1
BRDEN0.4auto	98.3	103.6	111.1	3.7	5.4	8.0
CNTRLPLAauto	129.3	139.8	146.1	1.5	2.2	4.3
BRPLA0.2auto	100.1	106.5	124.5	3.1	4.4	6.2
BRPLA0.4auto	104.0	110.0	117.1	1.9	4.5	6.5
BRDENsub	61.1	111.1	130.6	0.1	0.7	6.8
BRPLAsub	0.0	0.1	0.3	0.0	0.0	0.0
BRDENsubauto	98.8	102.5	113.9	2.9	5.0	7.5
BRPLAsubauto	0.2	22.5	94.6	0.0	0.1	0.5
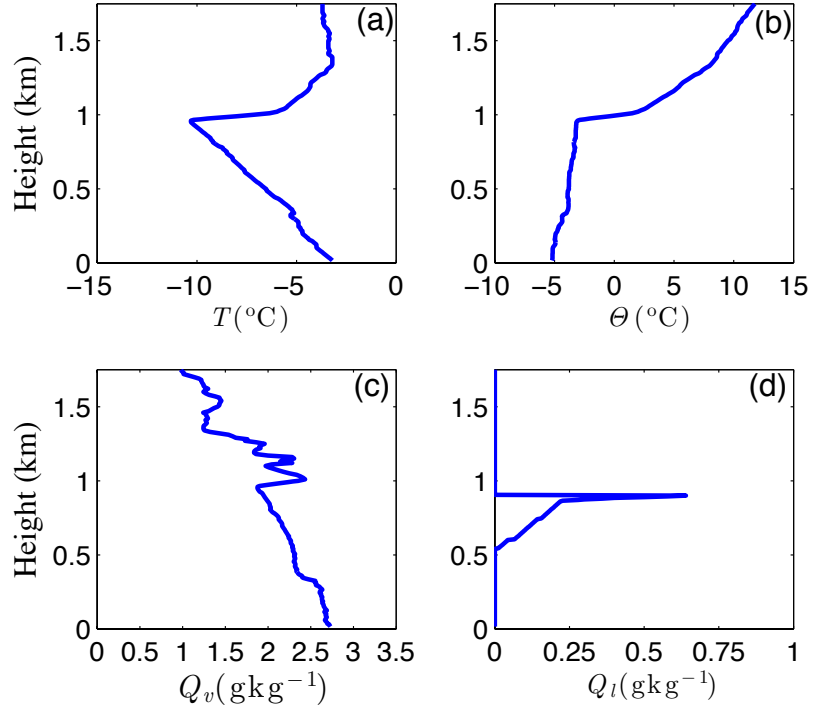
 Figures:

Figure 1: Radiosonde profiles of (a) temperature (*T*), (b) potential temperature (*Θ*), and (c)
specific humitidy (Q_v) used to initialize the LES. The profile of cloud liquid (Q_l) in panel (d) is
integrated from radiometer measurements.
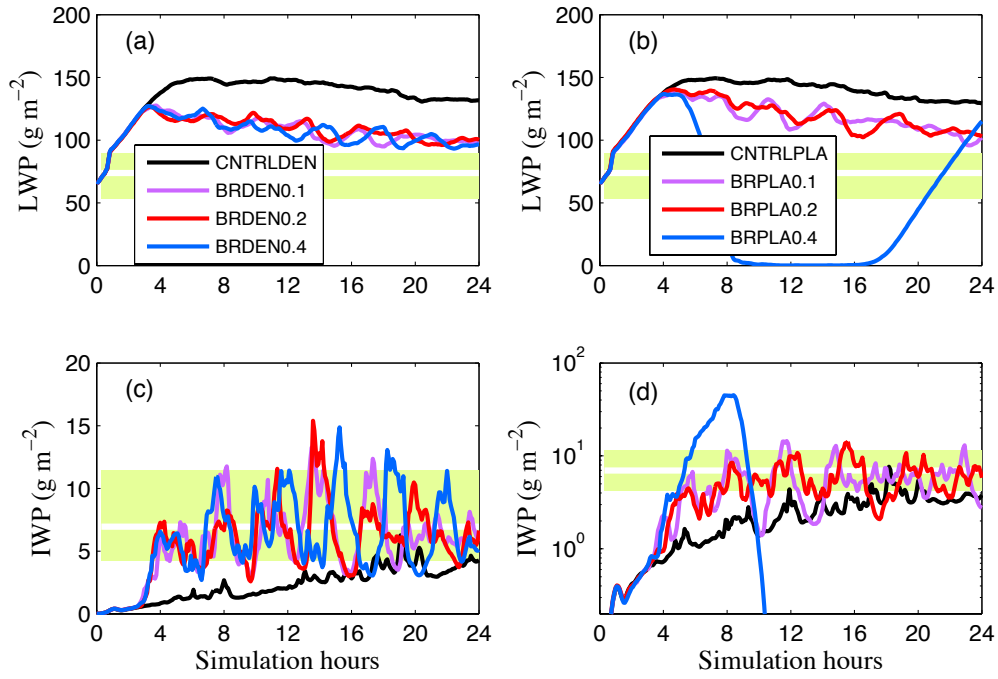
Figure 2: Timeseries of (a, b) LWP and (c, d) IWP for simulations with (a, c) dendrites and (b, d) plates. Light green shaded area indicates the interquartile range of observations, while the horizontal white line shows median observed values. Black lines represent simulations that account only for PIP. Purple, red and blue lines represent simulations with active break-up and a prescribed rimed fraction of 0.1, 0.2 and 0.4, respectively, for the cloud ice/snowflakes that undergo break-up. Note the logarithmic y-scale in panel (d).
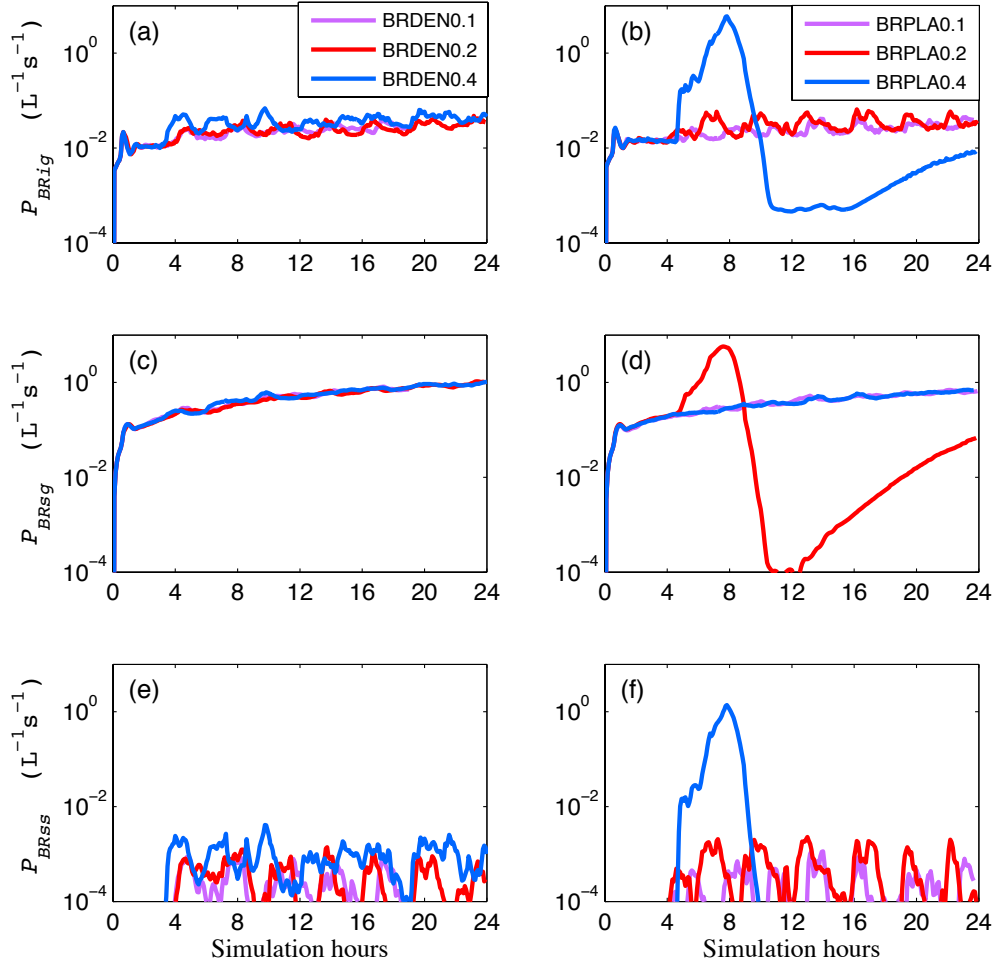
Figure 3: Timeseries of domain-averaged fragment generation rate (L^{-1}s^{-1}) from (a, b) cloud ice-graupel (P_{BRig}), (c, d) snow-graupel (P_{BRsg}) and (e, f) snow-snow (P_{BRss}) collisions, for simulations with varying rimed fractions for cloud ice/snow: 0.1 (purple), 0.2 (magenta), 0.4 (blue). Panels (a, c, e) correspond to simulations with dendrites, while (b, d, f) with plates. Note the logarithmic y-scale.

100

105

110
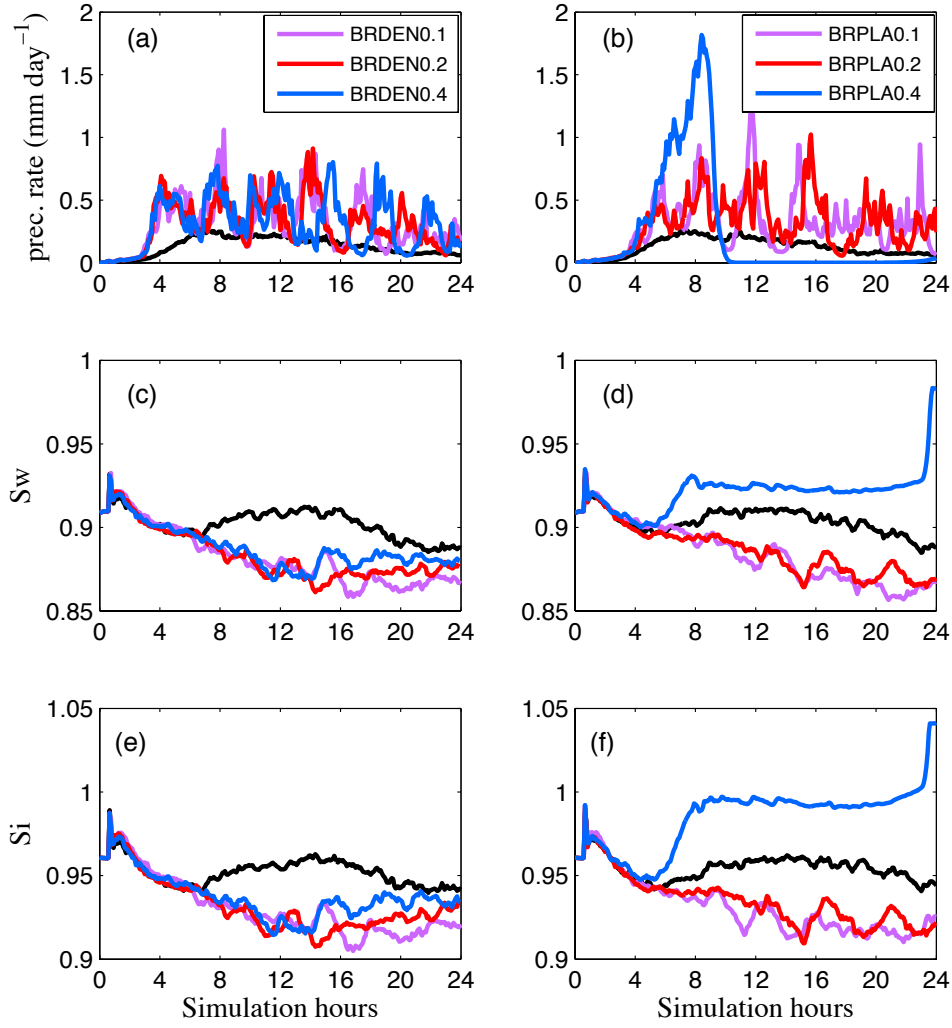
Figure 4: Timeseries of domain-averaged (a, b) surface precipitation rate (mm day^{-1}) and sub-cloud minimum saturation with respect to (c, d) water and (e, f) ice. Black line corresponds to simulation without active break-up. In the rest of the simulations, rimed fraction is set to 0.1 (purple), 0.2 (magenta) and 0.4 (blue). Panels (a, c, e) correspond to simulations with dendrites, while (b, d, f) with plates.
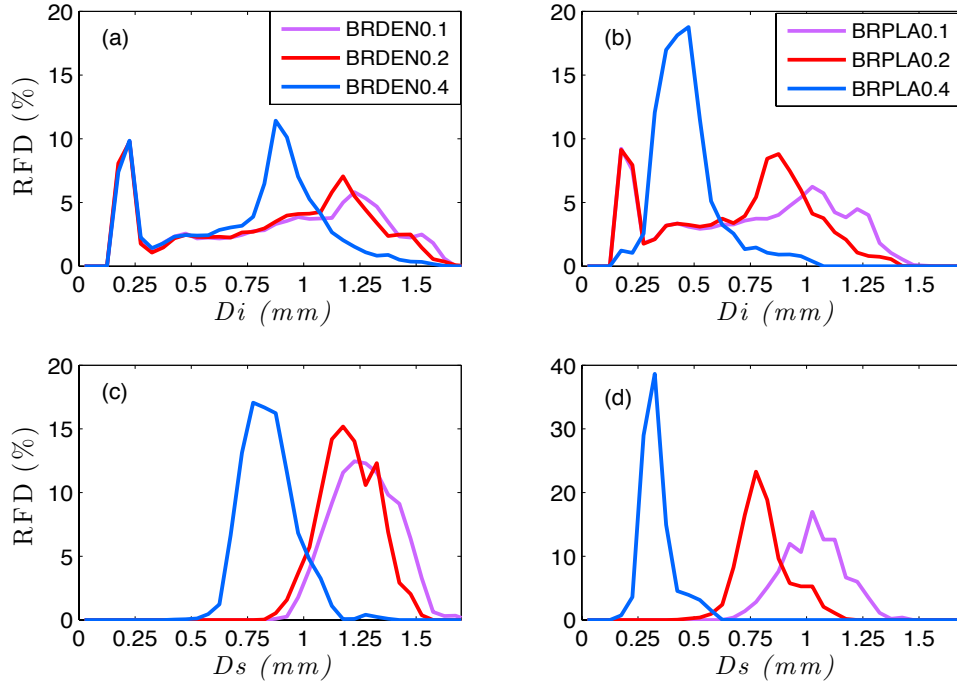
Figure 5 : Relative Frequency Distribution (RFD) of the mean (a, b) cloud ice and (c, d) snow diameter for simulations with (a, c) dendrites and (b, d) plates. Purple, red and blue lines correspond to a prescribed rimed fraction of 0.1, 0.2 and 0.4 for the cloud ice and snow particles than undergo break-up. Calculations are performed offline based on the domain-averaged cloud ice and snow concentrations.
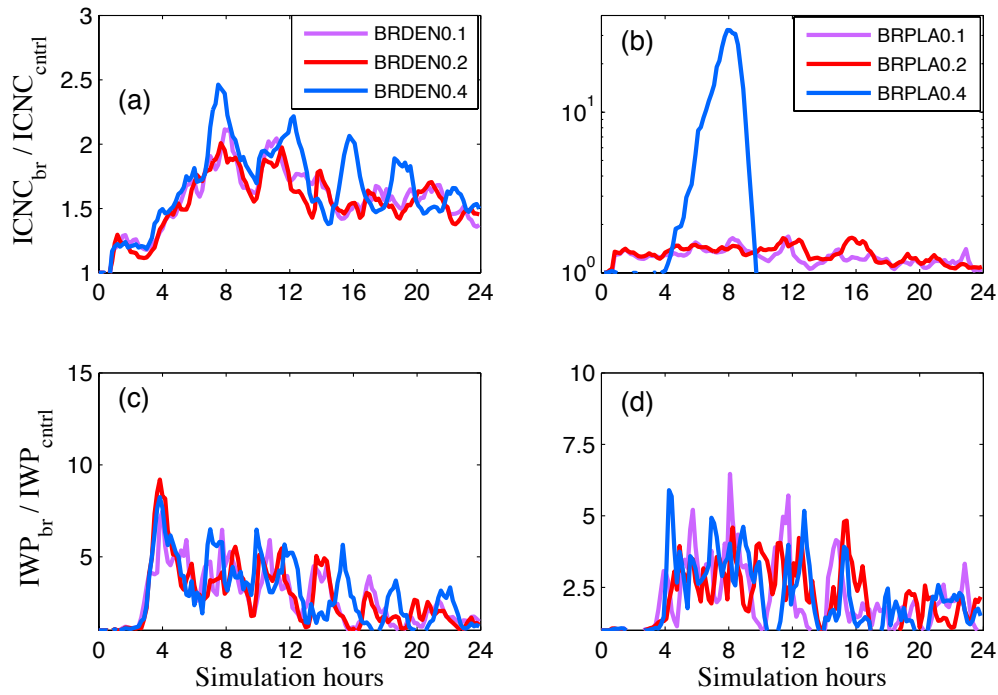
Figure 6: Timeseries of domain-averaged (a, b) ICNC and (c, d) IWP enhancement due to break-up. ICNC (IWP) enhancement is calculated by dividing the total ICNCs produced in each simulation with active ice multiplication with those produced by the control experiment that accounts only for PIP. The rimed fraction of cloud ice/snowflakes that undergo break-up is set to 0.1 (purple), 0.2 (magenta) and 0.4 (blue). Panels (a, c) correspond to simulations with dendrites, while (b, d) with plates.

165
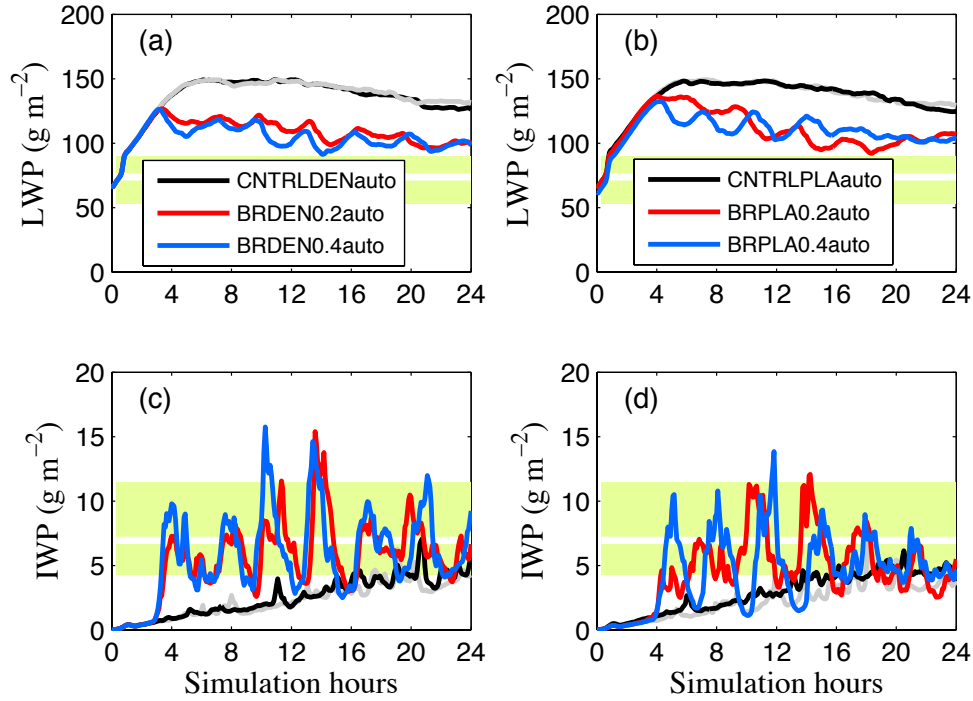
Figure 7: Same as Figure 2 but for simulations with active cloud ice-to-snow autoconversion. The cloud ice habit is set to (a, c) dendrites and (b, d) plates. Black lines represent simulations that account only for PIP. Red lines include the break-up process with a prescribed rimed fraction for cloud

170 ice/snow set to 0.2. Blue lines are similar to red but with the prescribed fraction set to 0.4. Light grey lines represent baseline simulations that do not account for autoconversion: (a, c) CNTRLDEN and (b, d) CNTRLPLA (see Table 3).

175

180
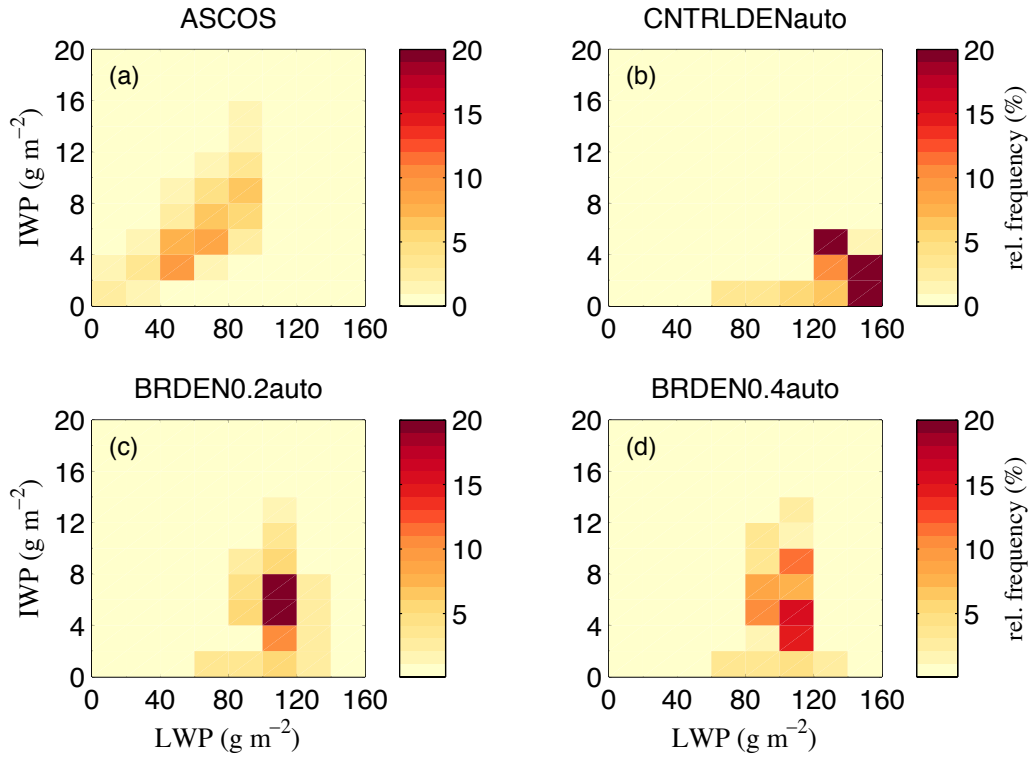
Figure 8: Relative frequency distribution of IWP (g m^{-2}) as a function of LWP (g m^{-2}) for (a) ASCOS, (b) CNTRLDENauto, (c) BRDEN0.2auto and (d) BRDEN0.4auto (see Table 3). Cloud ice-to-snow autoconversion is active in all model simulations. Collisional break-up is included only in panels (c-d) with the cloud ice/snow rimed fraction set to (c) 0.2 and (d) 0.4. In all simulations a dendritic cloud ice habit is assumed.
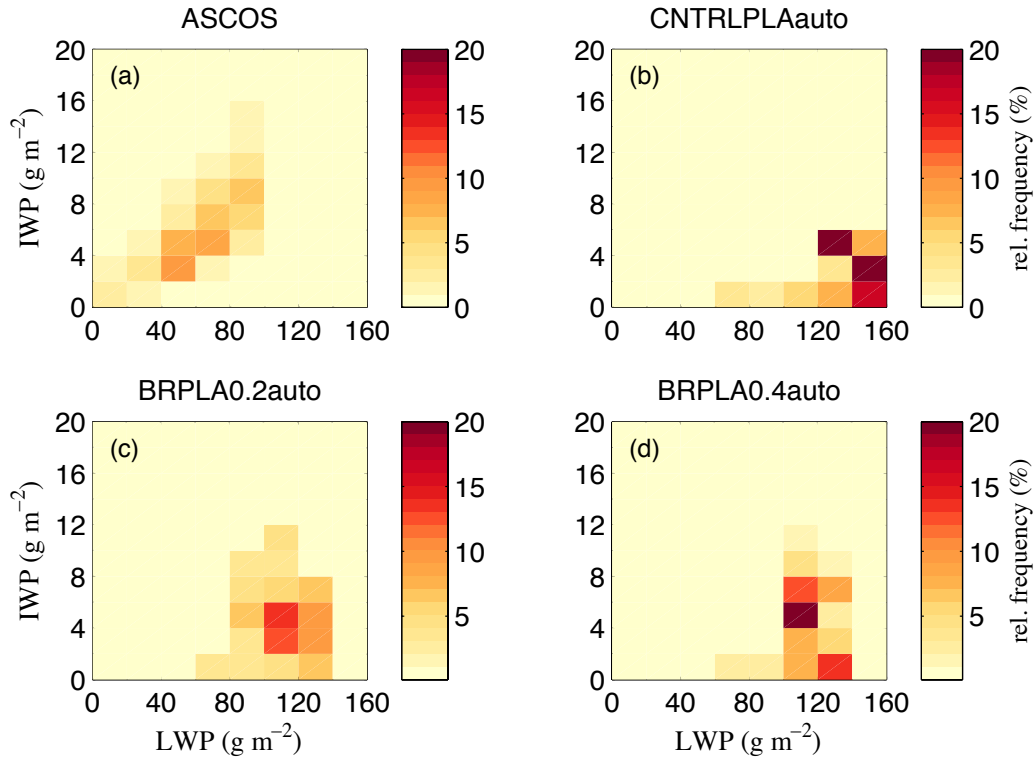
Figure 9: Relative frequency distribution of IWP ($g m^{-2}$) as a function of LWP ($g m^{-2}$) for (a) ASCOS, (b) CNTRLPLA, (c) BRPLA0.2auto and (d) BRPLA0.4auto (see Table 3). The set-up in each panel is similar to Fig. 8, except that in all simulations a planar cloud ice habit is assumed.
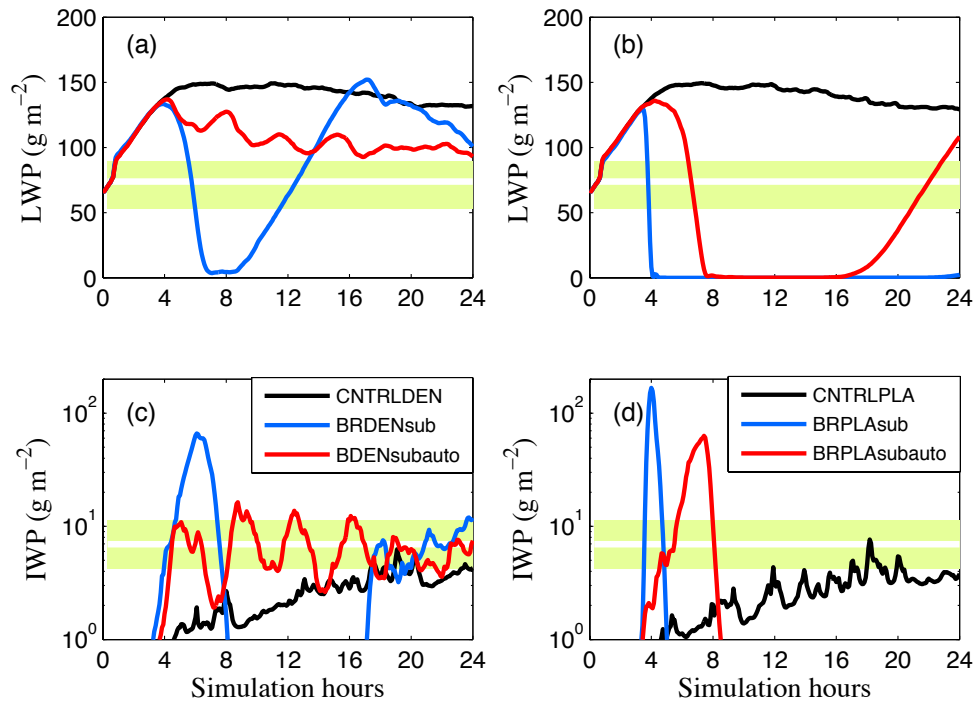
Figure 10: Similar to Fig. 2 but for simulations that do not include the sublimation correction factor in the break-up parameterization. Cloud-ice to snow autoconversion is active in BRDENsubauto and BRPLAsubauto simulations. Rimed fraction is set to 0.2.